Chapter 6

Current channeling distortion analysis

Besides analyzing the dimensionality of the MT data, another goal is to find out whether part of the region can be explained with a 2-D regional model overlain by local, shallow, horizontally elongated conductors oriented differently. I will refer to this model as the channeling model, where the regional electric fields are strongly distorted and polarized in one single direction due to a high concentration of currents that are channeled by the local conductors (current channeling effect; section 6.1).

The development of the methodology (theory in section 6.1 and test of the hypothesis in section 6.2) was stimulated by the observation that our measured MT data from several sites show impedance phases of the coast parallel (∼N-S) electric field component (TE-polarisation mode) surpassing 90°, manifesting therefore a common strong distortion effect (section 6.3). It was impossible to determine a consistent regional strike (section 6.3.1). The data are seen to be affected by strong current channeling, especially in the near coast region where the conductive ocean has an important influence with regard to enhancing the current flow upon crustal thin vertical dike-type conductors, if these are oriented sub-parallel to the coast line (section 6.2). Thereby the TE-polarization mode is the most affected by the channeling.

The presented analysis serves also as an important tool to recognize qualitatively high conductivity anomalies, by imaging the 3-D induction strength parameters (section 6.1.8), the current channeling misfit (section 6.1.10) and the average magnetic parameters (section 6.3.2). The images serve to scrutinize if a 2-D model is reliable or if a 3-D modeling is necessary for the region, as well as to allow an identification of current channeling effects (section 6.3.3). Thereby the anomalies are identified and are considered as *a priori* information for the construction of the forward 3-D models (Chapters 7 and 8).

The current channeling analysis allowed indeed the inference of the presence of elongated conductor(s) oriented mostly in NNW-SSE direction in the Coastal Cordillera, which can be correlated with the Atacama fault system (section 6.3.3). In the forearc region further from the ocean (Precordillera), elongated conductors oriented in ∼N-S directions were also

identified, and can be associated with the Precordillera fault system where the West Fissure is located (section 6.3.3). However, a strong 3-D inductive effect is observed in this region (section 6.3.2), and is interpreted as being due to a coupling between shallow 3-D anomalies and a deeper conductive layer (chapter 8).

In addition, the channeling analysis applied to the data and to the model responses of 3-D models allows an explanation for the phases >90° (Chapters 7 and 8).

6.1 Presentation of the theory

Based on the 2-D superposition model (Chapter 1.2), where telluric and magnetic galvanic distortions produced by local 3-D anomalies affect the regional fields (section 1.2.6), in the following is presented a tensor distortion analysis method which deals with the case of local strong current channeling. This effect is understood as a strong flow of DC (direct current)-lines channeled by local conductivity structures. The term "channeling" refers to a higher current density in one certain direction (x): $J_x = \sigma_1 \mathbf{E_x}$, where σ is the conductivity of the medium and E_x the electric field in it. To have a stronger current flow in one preferable direction will depend of course on the conductivity distribution. Several authors have discussed the possible reasons for the current channeling (e.g., Babaour and Mosnier [1980]). This has been reviewed in a paper by Jones [1983], where the effect is explained as a high concentration of currents induced 'elsewhere' by external source fields, and are channeled by local conductors in a frequency independent ohmic-like manner (i.e., anomalous DC-currents). The term 'elsewhere' refers not to a conductivity structure which is the channeller itself (i.e., the local conductor), but rather to the region causing the currents that will be trapped by the local conductors. For the channeling model presented here, the currents induced elsewhere can be thought to be from the regional 2-D structure, whereas the channeller is assumed to be horizontal elongated conductors oriented differently with respect to the regional strike. Given the different strike angle between the regional and local structure, the currents channeled in the latter are "anomalous" in the sense that these deviate and deform the regional electric fields (by a twist and shear distortion angles; Groom and Bailey [1989a]).

As will be shown later, a horizontal elongated conductor alone induces a higher current density along its long axis. If in addition currents induced elsewhere exist, these can contribute to enhance the current density in the conductor, leading to a strong local current channeling effect.

To achieve DC-currents, the penetration depth of the fields must be larger than the thickness of the elongated conductors (e.g., Jones [1983]). On the other hand, higher current flows can increase the anomalous DC magnetic fields; therefore to account for galvanic magnetic distortions the distorted tensor was expressed in terms of a matrix of complex numbers (section 6.1.1) in order to include them further in the current channeling analysis.

A simple model to reproduce linear currents along a horizontal axis is a shallow, horizontally elongated, good conductor (σ_1) embedded in a resistive space (e.g., McNeill and Labson [1987]). Kaufman and Keller [1981] estimated an analytical function for the ratio of current density inside and outside a conductive horizontal spheroid as a function of its ellipticity e

(long and short radios a, b) and conductivity contrast (σ_1/σ_2). This function is expressed in terms of a "depolarization factor" L estimated from the electric potential function inside and outside the anomaly, for a primary electric field ($E_0 x$) aligned to the principal axis (TE-polarisation). The depolarization factor L represents the effect of surface charges and has the expression:

$$L = \frac{1 - e^2}{2e^2} \ln(\frac{1 + e}{1 - e} - 2e)$$

where $e = [1 - (b^2/a^2)]$. Note that L decreases with the ellipticity, vanishing at an infinite elongation.

The electric field inside the spheroid (E_{ix}) can be expressed as function of the depolarization factor (L):

$$E_{ix} = \frac{E_{0x}}{1 + [\frac{\sigma_1}{\sigma_2} - 1]L} \tag{6.1}$$

which is uniform and directed along the long axis (x), and it approaches the primary field (E_{0x}) as $L \ll 1$, while it decreases as σ_1/σ_2 increases (fig.6.1a).

From the above expression the current density inside the conductor is $j_x = \sigma_1 E_{ix}$, whereas outside the body it is $\sigma_2 E_{0x}$. This indicates that the current density in the local body increases with higher conductivity contrast (between the body and the regional space) as well as with the length (a) of the body for observations realized near its center and at periods where the skin depth δ_1 (in terms of the body material) satisfies $b/\delta_1 \ll 1$ in order to approach the electrostatic effect (DC-currents).

For long anomalies ($a \gg b$), as the conductivity contrast σ_1/σ_2 increases, the current density and the corresponding magnetic field intensity linearly increase with σ_1 until the currents saturate at an extreme conductivity contrast (McNeill and Labson [1987]). With further increase of σ_1 the electric field E_i becomes smaller (6.1). Furthermore, Kaufman and Keller (1981) showed that for observations above the body the horizontal (and vertical) anomalous magnetic field (normalized by the primary field) increases exponentially with the ratio a/b at high conductivity contrasts ($\sigma_1/\sigma_2 > 10^3$), when the skin depth in the material is much larger than the body thickness (b).

The EM-response of an elongated spheroid is similar to that of a vertical dike-type conductor provided that both have similar width and length, and similar ratio b/δ, where b is the height of the body and δ its skin depth. This is due to the principle of quasi-equivalence ruled by the electromagnetic induction (of limited penetration depths), which leads to the non-unique solution in regard to different models having equivalent responses.

A numerical example is shown for the horizontal electromagnetic field responses of a dike-type conductor (fig.6.1), tested for different lengths (a) and a fixed resistivity contrast of 1/1000 (with diffuse boundaries). The dike (1 Ωm) is 8 km thick and 10 km deep.

For the electric field amplitude aligned to the long axis ($|E_x|$ normalised; inside the page in fig.6.1a), the distortion of the primary field (i.e., a drop of its amplitude due to the dike) broadens horizontally with increase in the length of the dike at all periods. At long periods, however, the effect of the dike to the electric field vanishes in the 2-D case, as predicted by the corresponding equation in terms of the depolarisation factor (eq.6.1). The more localised distortion effect by the shorter dikes reflects the "edge effect" of the charges concentrated at the end of its boundaries. These surface charges attenuate the electric field intensity $|E_x|$ even

at long periods, where the effect broadens (in terms of the horizontal distance from the dike) with increasing length of the dike (fig.6.1a). The reduction of $|E_x|$ in the surface surrounding regions of the dike will be the basal assumption for the channeling model hypothesis (sections 6.1.3, 6.1.4).

The intensity of the anomalous magnetic field across the dike ($|B_y|$ normalised; fig.6.1b) increases and broadens with the length of the dike at all period. Its intensity decreases with the period but increases with the length of the dike.

The distortion of the electric field across the dike (($|E_y|$ normalised; fig.6.1c) approaches a static shift effect (i.e., independent of period) for observations above the anomaly. The dependence of the anomalous fields on the length of the dike and the period is seen only at the dike boundaries where the field is up-shifted, but it returns to the primary field values at long periods. This up-shifting behaviour is indicative of induction at short periods, where the skin depth (p in km ; fig.6.1) is not much larger than the scale of the dike. The induction is also stronger by shorter dikes.

It has been demonstrated that a small dike alone embedded in a homogeneous resistive space can produce strong intensity variations in the primary fields. The current density can be magnified (or reduced) with an additional conductivity structure, such as a regional conductor contributing to the current flow in the dike (i.e, induced elsewhere as outlined previously).

The elongated anomaly (or distorter) is assumed to consist of a shallow thin vertical dike-type conductor embedded in a 2-D regional space, provided that the host medium in which the dike lies is much more resistive than it, thus enhancing the electrostatic current flow. The anomaly is oriented in a different local azimuth with regard to the regional strike. The anomalous EM fields can be subtracted from the total fields (i.e., recovering of the regional response) if the regional conductivity contrast is electrically far enough away from the observation point so as to achieve the condition of uniform background (regional) fields in the dike(s), the hypothesis on which the superposition model is based (Chapter 1.2).

Based on the above defined model of a vertical highly conductive dike of limited lateral extensions as the channeler, the EM-field boundary conditions between the different domains (dike and host) contribute to the current channeling analysis (6.1.3). The idea is to detect the presence of the anomalous currents, and quantify its effect on the horizontal components of the regional electric and magnetic fields (section 6.1.4). Then, the direction (or the local azimuth) of the anomaly that channels the currents can be determined (section 6.1.5). By small angle differences between local and regional strikes a particular distortion effect arises, namely that anomalous magnetic effects are only distinguishable by the TE-(tangential electric) polarisation mode (section 6.1.6). If DC-currents (i.e., galvanic) predominate over induction, the regional 2-D information can be recovered (section 6.1.7), provided also that the regional fields are uniform inside the anomaly.

The parameters useful for the current channeling analysis are summarized in sections 6.1.8 - 6.1.10, which are plotted or extrapolated for their 3-D images to identify the anomalous conductivity structures (sections 6.3.2, 6.3.3).
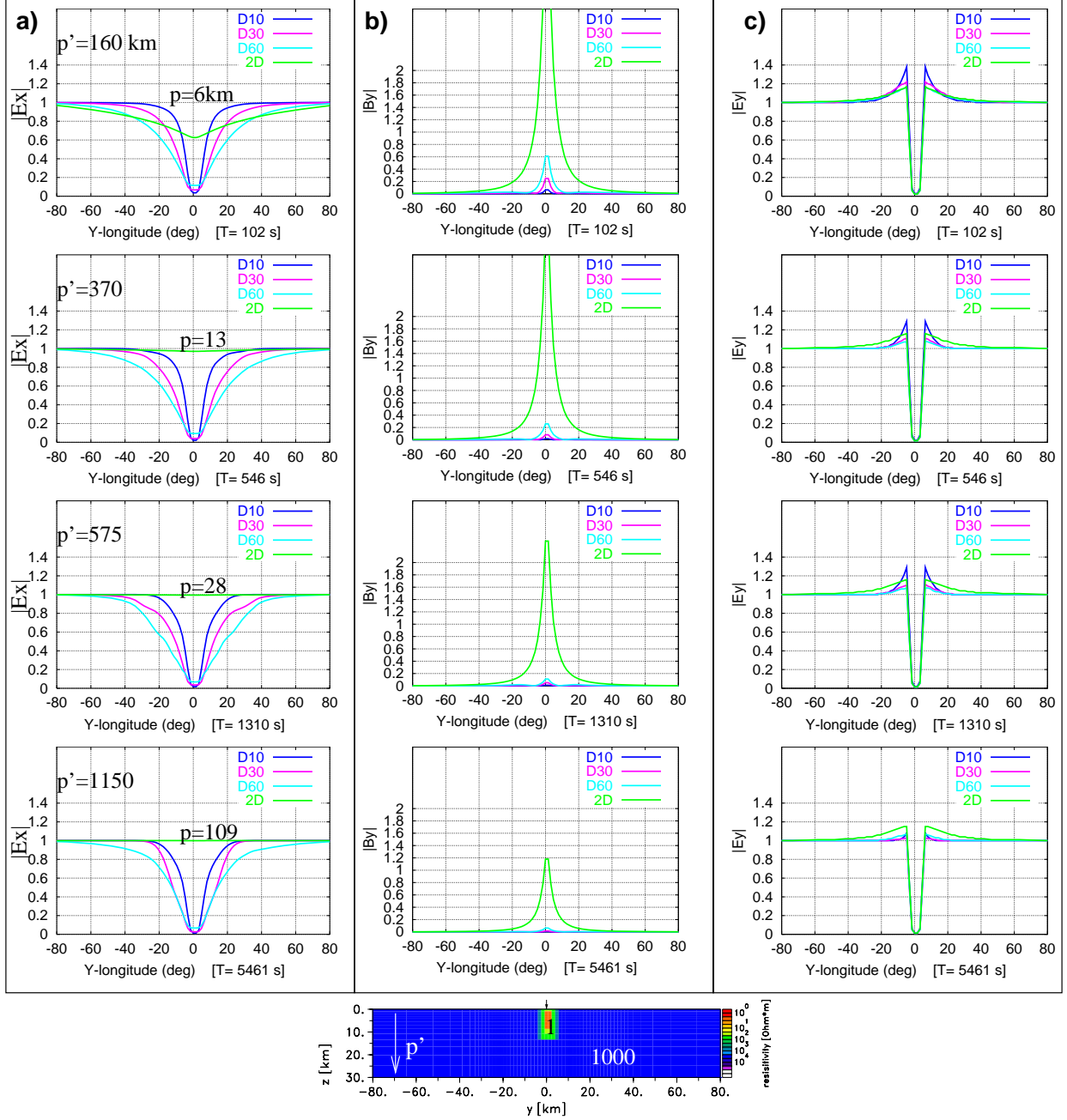
Figure 6.1: Horizontal electromagnetic field responses of a vertical conductive dike (1 Ω.m; 10x10 km^2) embedded in a homogeneous resistive space (1000 Ω.m). The length of the dike (x, into the page; model below) was variably tested; 10 (D10), 30 (D30), 60 km (D60) and infinite (2D) long. *a)*: Amplitude of the electric field along the dike ($|E_x|$). Also shown are the corresponding skin depths (in km) in the resistive medium (p') and in the dike (p). *b)*: Amplitude of the anomalous magnetic field across the dike ($|B_y|$). *c)*: Electric field intensity of the component across the dike ($|E_y|$). From top to bottom are shown different periods (100, 550, 1300 and 5500 s), representative of increasing penetration depths (skin depths in column *a*). The amplitudes are normalised to their respective primary fields.

69

6.1.1   A complex matrix of the galvanic telluric and magnetic distortions

Using Smith's (1997) expression for the telluric and magnetic tensor decomposition introduced in section 1.2.6 (eq.1.24), it is seen that the term $(D_e - \mathbf{Z}\,D_m)^1$ is a matrix of complex numbers which can be identified as the unique distortion matrix of the electrostatic effect. This unique matrix, which is a function of the magnetic $(\gamma,\,\varepsilon)$ and telluric $(b,\,c)$ distortion parameters and of the elements of the measured $\mathbf{Z}$, is associated with a *complex distortion matrix* C in the form:

$$C = (D_e - \mathbf{Z}\,D_m) = \begin{bmatrix} ge^{i\vartheta} & re^{i\beta} \\ te^{i\alpha} & we^{i\delta} \end{bmatrix} \tag{6.2}$$

Note the the distortion matrix C is frequency dependent since the measured tensor $\mathbf{Z}$ is contained in it.

The distorted (i.e., measured) impedance tensor in the regional coordinate system is

$$\mathbf{Z} = C\mathbf{Z^r} = \begin{bmatrix} rZ_{yx}^r e^{i\beta} & gZ_{xy}^r e^{i\vartheta} \\ wZ_{yx}^r e^{i\delta} & tZ_{xy}^r e^{i\alpha} \end{bmatrix}. \tag{6.3}$$

From this expression it is observed that each pair of column tensor elements (involved in their respective telluric vectors; Bahr [1988]) will no longer have equal phases. The values β, δ and α, ϑ are the "phase deviations" from the regional phases ϕ_{yx}^r and ϕ_{xy}^r, respectively, which are related to the magnetic distortion effects.

The relation between the complex matrix C and the telluric and magnetic distortion matrices $D_{e,m}$ is seen by associating eq.(1.24) with eq.(6.3):

$$\begin{aligned} Z_{xx} &= (c - \varepsilon Z_{xy})\,Z_{yx}^r = \left(re^{i\beta}\right) Z_{yx}^r \\ Z_{yx} &= (1 - \varepsilon Z_{yy})\,Z_{yx}^r = \left(we^{i\delta}\right) Z_{yx}^r \\ Z_{xy} &= (1 - \gamma Z_{xx})\,Z_{xy}^r = \left(ge^{i\vartheta}\right) Z_{xy}^r \\ Z_{yy} &= (b - \gamma Z_{yx})\,Z_{xy}^r = \left(te^{i\alpha}\right) Z_{xy}^r. \end{aligned} \tag{6.4}$$

From there we can quantify the observed impedance phase deviations from the regional response. For example, the phase deviation of Z_{xy} with respect to the regional phase Z_{xy}^r is

$$\vartheta = \arctan\left(\frac{-\gamma\,\mathrm{Im}\,Z_{xx}}{1 - \gamma\,\mathrm{Re}\,Z_{xx}}\right).$$

Then the total measured phase is: $\phi_{xy} = \vartheta + \phi_{xy}^r$, where the regional phase is $\phi_{xy}^r = \arctan\left(\frac{\mathrm{Im}\,Z_{xy}^r}{\mathrm{Re}\,Z_{xy}^r}\right)$.

---

[1]The telluric and magnetic distortion matrices are: $D_e = \begin{matrix} 1 & c \\ b & 1 \end{matrix}$, $D_m = \begin{matrix} \gamma & 0 \\ 0 & \varepsilon \end{matrix}$, respectively.
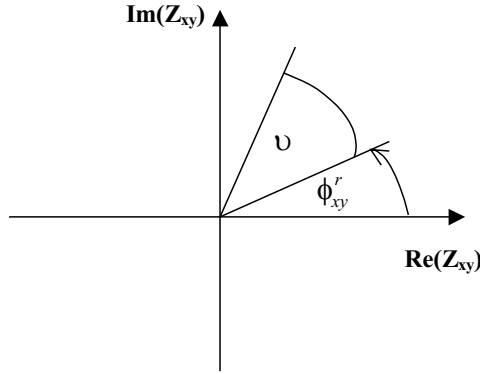
Figure 6.2:
Graphical representation of the phase deviation ϑ arising from the magnetic effects. The distorted measured phase is the sum of ϑ and the regional phase ϕ_{xy}^r .

The complex distortion parameters of the matrix C can be determined from the exact solutions given by Smith [1997] for the distortion parameters b, c, ε and γ (section eqs. 1.26, 1.27), provided that the regional strike is known. Then the estimated distortion parameters are introduced in eq.6.4. Since the measured impedance $\mathbf{Z}$ is known (assumed in the regional coordinate system), the elements of the matrix C (eq.6.2) can be recovered from the equation.

6.1.2 Relation with the telluric tensor decomposition

The twist and shear angles of the Groom & Bailey (1989) telluric tensor decomposition (eq.1.18) can be expressed directly in terms of the tensor element quotients −identified as the telluric vector angular deviations (Bahr [1991])− in the form:

$$
\begin{aligned}
\beta_e + \beta_t &= \arctan(\frac{Z_{yy}}{Z_{xy}}) \\
\beta_e - \beta_t &= \arctan(\frac{Z_{xx}}{Z_{yx}})
\end{aligned}
\tag{6.5}
$$

This relationship is obtained from eq.(1.20) and by considering the arc-tangent function property of variable summation (see Appendix. B.1).
By considering eq.(6.4), the above twist and shear relations in terms of the complex distortion parameters are:

$$
\begin{aligned}
\beta_e + \beta_t &= \arctan\left(\frac{t}{g}e^{i(\alpha-\vartheta)}\right) \\
\beta_e - \beta_t &= \arctan\left(\frac{r}{w}e^{i(\beta-\delta)}\right)
\end{aligned}
\tag{6.6}
$$

Thus, both distortion angles $(\beta_{t,e})$ are no longer real numbers, obviously due to the DC magnetic effects.
In the case of similar phase deviations between each tensor element pair (i.e., $\alpha \approx \vartheta$, $\beta \approx \delta$), twist and shear will be approximately real numbers. This special

case indicates that certain symmetrical magnetic effects will not be detectable by a telluric galvanic decomposition scheme and therefore the magnetic effect would be "absorbed" into the regional phases.

It will be demonstrated in the next section (6.1.4) that equal phase deviations occur under strong current channeling conditions, where magnetic distortion effects are not necessarily negligible.

6.1.3   The model affected by current channeling

This section is focused on the empirical study of the strong current channeling produced by a local shallow elongated conductor in the form of a thin vertical dike (fig.6.3). The long strike axis (x) of the anomaly coordinate system will be assigned as the "local azimuth".

The physical meaning of this special distortion can be explained by the boundary conditions accomplished for the electromagnetic fields intersecting two different conductivity spaces, in which space 1, represented as the shallow elongated anomaly, has a very high conductivity value (σ_1), while space 2, the regional electrical structure, is resistive (with conductivity σ_2; figs.6.3). As was introduced at the beginning of this chapter, inasmuch the conductivity contrast increases (σ_1/σ_2) the current density will strengthen too.

Also, we are interested in the fields located near the centre of the anomaly in order to examine current lines along the x-axis, valid obviously for an anomaly which is much longer than wide (i.e., high ellipticity in case of a spheroid). The anomaly should be also electrically thin (in regard to the field penetration depths in the anomaly) so as to neglect induction effects and therefore the electrostatic effect prevails (DC-currents effecting the regional fields). In addition, the background EM-fields (from the regional structure) are assumed uniform in the anomaly (i.e, as primary fields) in order to achieve valid boundary conditions between two domains (the anomaly and the host).

For incident EM plane waves at the earth surface and under the approach assumed for the electromagnetic induction in the earth by the MT sounding (section 1.1), the boundary conditions (BC) set by the electric ($\mathbf{E_{1,2}}$) and magnetic ($B_{1,2}$) fields at an interface between domains of different electrical conductivities (σ_1, σ_2) are:

1) $\hat{n} \cdot (\sigma_2 \mathbf{E_2} - \sigma_1 \mathbf{E_1}) = 0$
2) $\hat{n} \times (\mathbf{E_2} - \mathbf{E_1}) = 0$
3) $\hat{n} \times (\mathbf{B_2} - \mathbf{B_1}) = 0$
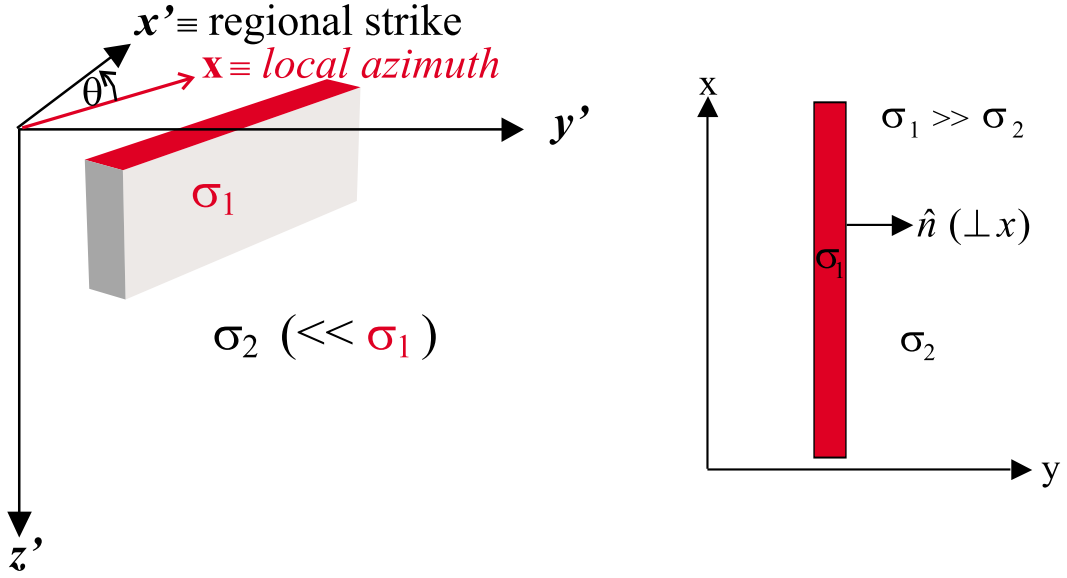*4)* $\hat{n} \cdot (\mathbf{B_2} - \mathbf{B_1}) = 0$

with $\hat{n}$ defining the unit vector normal to the interface.

From BC *1)* the following is observed (fig.6.4) for the electric fields at the interface:

If $\sigma_1 > \sigma_2 \ \Rightarrow \ \hat{n} \cdot \mathbf{E_2} > \ \hat{n} \cdot \mathbf{E_1}$

Thus, the electric field across the dike (i.e., the normal component E_y; Fig.6.4) will jump at the boundary being down shifted in the conductive space. For electrically thin vertical

Figure 6.3: The channeling model represented by a shallow thin vertical dike-type conductor, which strikes along x −the local azimuth−, and is embedded in a regional space of coordinate system x'-y'. *Left:* 3-D view of the anomaly and the regional space. θ is the angle between both principal axes (x, x'). *Right:* Horizontal view of the anomaly in the local azimuth coordinate system. $\hat{n}$ is the component normal to the dike. Model valid for skin depths (in the dike) much larger than the thickness of the dike.

dikes (thickness/$\delta < 1$) however the electric field will suffer a very local variation, namely just above the thin anomaly, while it jumps up immediately near its boundaries and returns to the normal field values further away from the anomaly (fig.6.4). Therefore from a regional point of view (with regard to the skin depth), the electric field across the thin dike remains almost constant, except for observations performed immediately above it (fig.6.1c).

Because the electric field intensity in a good conductor reduces in magnitude (figs. 6.4, 6.5), the following can be deduced from BC 1 and BC 2)[2]:

If $\sigma_1 \gg \sigma_2$ then $\quad |\mathbf{E_1}| \ll |\mathbf{E_2}| \quad \Rightarrow \quad \hat{n} \times \mathbf{E_2} \ll \hat{n} \cdot \mathbf{E_2}$

i.e., the electric field component parallel to the boundary ($\hat{n} \times \mathbf{E_2}$) reduces considerably in magnitude compared to the normal field component outside the dike ($\hat{n} \cdot \mathbf{E_2}$) due to a high conductivity contrast.

Considering BC *1)*, which implies continuity of the current flow across the boundary (Fig.6.4), and applying Ampere's law for this current flow results in a constant magnetic field of the component parallel to the boundary ($\hat{n} \times \mathbf{B_{1,2}}$). This is the well known condition observed in the TM-polarization mode in the case of two dimensionality; the magnetic field on the surface shows no variation as function of space, whereas the electric field does (E_y in Fig.6.4).

With Biot-Savart's law of the current flow along the elongated anomaly and BC *2)*, the magnetic field across the anomaly (normal component; Fig.6.4) increases in magnitude. In other words, because the tangential electric field ($\hat{n} \times \mathbf{E_{1,2}}$) varies continuously across the boundary, the current density must jump at the interface, showing an increase in the high

---

[2]in a perfect conductor, the electric field vanishes

conductivity region. Therefore, the magnetic field perpendicular to the boundary ($\hat{n} \cdot \mathbf{B_{1,2}}$) increases in the conductive region, too. This occurs in the TE-polarization mode of a two dimensional space.
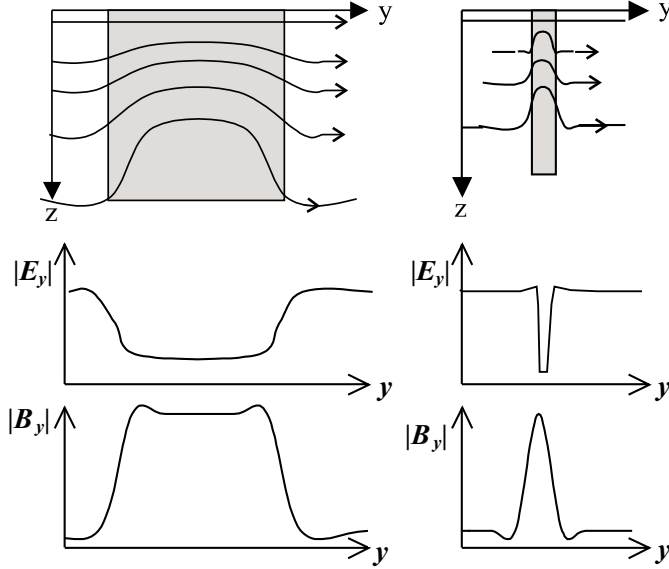

Figure 6.4:
Above: Current flow across spaces with laterally different conductivities. *Below:* Electric and magnetic field amplitudes (normalised by the primary field) across the electrical heterogeneity. For an electrically thin conductive dike (right) the electric field suffers a very local shift down, whereas the magnetic component increases in the conductive region and its surrounding regions. (modified figure after McNeill & Labson, 1991). Observation valid for skin depths larger than the anomaly thickness.
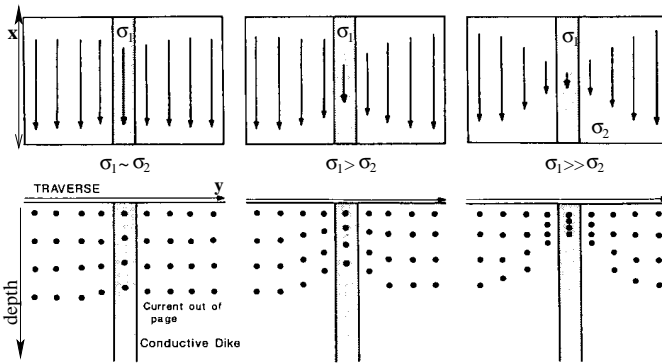

Figure 6.5:
The electric field E_x along a horizontally elongated conductor (*top*) will decrease in magnitude with increasing conductivity contrast σ_1/σ_2. *Bottom:* Vertical cross-section showing current flow concentration (after McNeill & Labson, 1991).

Distortion by a highly conductive thin vertical dike

How does a shallow vertical dike-type conductor affect the 2-D regional EM-fields? For those observations made above the regional host and placed close to the anomaly boundary, which consider the EM-field components *aligned with the axis of the anomaly* of penetration depths greater than the depth of the dike, the following conditions are found:

A) The *tangential electric field* reduces considerably in magnitude with respect to the background (primary) fields (fig.6.5; right and fig.6.1a) while the electric field perpendicular to the strike of the anomaly either increases or remains constant (fig.6.4; right and fig.6.1c).

B) The *anomalous magnetic field* is mostly perpendicular to the boundary surface (if magnetic effects are significant), i.e., the horizontal component (B_y; fig.6.4 and fig.6.1b) is *perpendicular* to the strike of the dike, the so called *local azimuth* direction.

Conditions **A**) and **B**) imply that the absolute value of the impedances Z_{xx}, Z_{xy} are very small because the observed electric field component parallel to the elongated conductor (i.e., along the x-axis) reduces considerably in magnitude, while the horizontal magnetic field amplitudes are either equal (for B_x) or higher (for B_y) with respect to the regional fields.

Therefore in the local azimuth coordinate system the elements of the impedance tensor

$$\mathbf{Z} = \left[\begin{array}{cc} Z_{xx} & Z_{xy} \\ Z_{yx} & Z_{yy} \end{array} \right]$$

can be approximated to:

$$Z_{xx} \ll Z_{yx} \quad Z_{xy} \ll Z_{yy}$$

which implies for the twist and shear relations written in Eqs. 6.5:

$$\begin{aligned} \beta_e + \beta_t &= \arctan(\frac{Z_{yy}}{Z_{xy}}) \approx \frac{\pm\pi}{2} \\ \beta_e - \beta_t &= \arctan(\frac{Z_{xx}}{Z_{yx}}) \approx 0° \end{aligned}$$

$$(6.7)$$

The above expression means that twist and shear distortion angles are maximal:

$$\beta_e = \beta_t \approx \pm\frac{\pi}{4}.$$

This approach has been also mentioned by Groom and Bailey [1989a] and Bahr [1991], in which they briefly assigned it to current channeling effects.
Expressed in terms of the telluric vectors[3] (Bahr [1988]):

$$\mathbf{e_x} = Z_{xx}\hat{x} + Z_{yx}\hat{y} \quad \approx \quad Z_{yx}\hat{y} \tag{6.8}$$

$$\mathbf{e_y} = Z_{xy}\hat{x} + Z_{yy}\hat{y} \quad \approx \quad Z_{yy}\hat{y} \tag{6.9}$$

It is seen that polarization *mode YX* (eq.(6.8)) behaves like in a *2-D induction* case. Only for polarization *mode XY* (eq.(6.9)) is the strong *current channeling* detectable (in the local azimuth coordinate system).

6.1.4   The distorted tensor of the channeling model

Solving the minimum value of the small tensor elements Z_{xx} and Z_{xy} of the local azimuth coordinate system −which correspond to the dropped electric field component aligned with the strike of the anomaly−, will allow the determination of the tensor distortion characteristics of the channeling model (i.e., of horizontally elongated conductors). For this, the two small

---

[3]The telluric vector $\mathbf{e_x}$ is the electric field induced by a magnetic field B_x which is linearly polarized in the x-direction. By analogy $\mathbf{e_y}$ is induced by a magnetic field B_y. In a 2-D model $\mathbf{e_x}$, $\mathbf{e_y}$ are perpendicular to B_x, B_y, corresponding to the YX and XY polarization modes, respectively.

impedance tensor elements will be expressed as functions of the distortion parameters of the complex matrix C:

$$C = \begin{bmatrix} ge^{i\vartheta} & re^{i\beta} \\ te^{i\alpha} & we^{i\delta} \end{bmatrix} \tag{6.10}$$

This matrix was defined in section 6.1.1 as the telluric and magnetic galvanic distortion of the regional impedance tensor, constituting the superposition 2-D model (eq.6.2). The observed tensor in the regional coordinate system (eq.6.3) is:

$$\mathbf{Z} = \begin{bmatrix} rZ^r_{y'x'}e^{i\beta} & gZ^r_{x'y'}e^{i\vartheta} \\ wZ^r_{y'x'}e^{i\delta} & tZ^r_{x'y'}e^{i\alpha} \end{bmatrix} \tag{6.11}$$

where $\mathbf{Z^r}$ denotes the regional tensor without local distortion and x',y' the regional coordinate system.

The tensor elements of the local azimuth coordinate system (x,y) is expressed as a function of the distorted tensor elements (eq.6.11) in the regional coordinate system (x',y') (see Appendix B.2 for details):

$$Z_{xy}(\theta) = \underbrace{\left\{ \sin\theta\cos\theta(re^{i\beta}) - \sin^2\theta(we^{i\delta}) \right\}}_{K_1} Z^r_{y'x'} + \underbrace{\left\{ \cos^2\theta(ge^{i\vartheta}) - \sin\theta\cos\theta(te^{i\alpha}) \right\}}_{K_2} Z^r_{x'y'} \tag{6.12}$$

$$Z_{xx}(\theta) = \underbrace{\left\{ \cos^2\theta(re^{i\beta}) - \sin\theta\cos\theta(we^{i\delta}) \right\}}_{L_1} Z^r_{y'x'} + \underbrace{\left\{ -\sin\theta\cos\theta(ge^{i\vartheta}) + \sin^2\theta(te^{i\alpha}) \right\}}_{L_2} Z^r_{x'y'} \tag{6.13}$$

where θ is defined as the angle between the local and the regional strike (positive c.c.w. with respect to the local conductor; fig.6.3) ranging between $-\pi/2$ and $\pi/2$.

The values of Z_{xy} and Z_{xx} are found as functions of the distortion parameters contained in the complex terms K_1, K_2 and L_1, L_2 of Eq.(6.12, 6.13), respectively (i.e., $r, w, g, t, \alpha, \beta, \delta \ and \ \vartheta$).

The element Z_{xy} approaches a minimum obviously when $Re(Z_{xy})$ and $Im(Z_{xy})$ do. Therefore, we treat real and imaginary parts of $Z_{xy}(\theta)$ separately and express them as functions of the complex numbers K_1 and K_2 defined in Eq.(6.12):

$$\begin{aligned} \mathrm{Re}\left\{ Z_{xy}(K_1, K_2) \right\} = {} & \mathrm{Re}\left\{ K_1 \right\} |Z^r_{y'x'}| \cos\phi^r_{y'x'} - \mathrm{Im}\left\{ K_1 \right\} |Z^r_{y'x'}| \sin\phi^r_{y'x'} \\ & + \mathrm{Re}\left\{ K_2 \right\} |Z^r_{x'y'}| \cos\phi^r_{x'y'} - \mathrm{Im}\left\{ K_2 \right\} |Z^r_{x'y'}| \sin\phi^r_{x'y'} \end{aligned} \tag{6.14}$$

$$\begin{aligned} \mathrm{Im}\left\{ Z_{xy}(K_1, K_2) \right\} = {} & \mathrm{Re}\left\{ K_1 \right\} |Z^r_{y'x'}| \sin\phi^r_{y'x'} + \mathrm{Im}\left\{ K_1 \right\} |Z^r_{y'x'}| \cos\phi^r_{y'x'} \\ & + \mathrm{Re}\left\{ K_2 \right\} |Z^r_{x'y'}| \sin\phi^r_{x'y'} + \mathrm{Im}\left\{ K_2 \right\} |Z^r_{x'y'}| \cos\phi^r_{x'y'} \end{aligned}$$

where $\phi^r_{x'y'}$, $\phi^r_{y'x'}$ are the regional phases of each polarization mode.

The solution is possible only by finding the zero-values of $Re, Im(K_1)$ and $Re, Im(K_2)$ independently (Eq.(6.14)) in order to fulfill the assumption of galvanic distortion (i.e., DC-currents). Considering $K_1 Z^r_{y'x'} + K_2 Z^r_{x'y'}$ together for a common minimal extreme value would imply that the regional impedances are modified by the distortion parameters, i.e., the anomaly exerts an inductive effect on the regional fields. Similarly, finding a minimal value for the function $Re, Im(K_1 Z^r_{y'x'})$ would imply an induction effect on the regional $Z^r_{y'x'}$ and, by analogy, the minimal value for $Re, Im(K_2 Z^r_{x'y'})$ would imply an induction effect on the regional $Z^r_{x'y'}$. The same situation is valid for the solution of Z_{xx}: $Re, Im(L_1)$ and $Re, Im(L_2)$ of Eq.(6.13) should be analyzed independently.

Then:

$$Re(K_1) = Re(L_1) = 0 \quad \Rightarrow \quad \tan(\theta) = \frac{r\cos\beta}{w\cos\delta}$$

$$Im(K_1) = Im(L_1) = 0 \quad \Rightarrow \quad \tan(\theta) = \frac{r\sin\beta}{w\sin\delta}$$

$$Re(K_2) = Re(L_2) = 0 \quad \Rightarrow \quad \tan(\theta) = \frac{g\cos\vartheta}{t\cos\alpha}$$

$$Im(K_2) = Im(L_2) = 0 \quad \Rightarrow \quad \tan(\theta) = \frac{g\sin\vartheta}{t\sin\alpha}$$

And the unique solution is:

$$
\left.\begin{array}{c}
|Z_{xy}(\theta)| \approx 0 \\
|Z_{xx}(\theta)| \approx 0
\end{array}\right\}
\qquad
\begin{array}{c}
\frac{r\cos\beta}{w\cos\delta} = \tan(\theta) = \frac{r\sin\beta}{w\sin\delta} \\
\frac{g\cos\vartheta}{t\cos\alpha} = \tan(\theta) = \frac{g\sin\vartheta}{t\sin\alpha}
\end{array}
\tag{6.15}
$$

which leads also to the following solutions for the other tensor elements in the local azimuth coordinate system (general expression in app. B.2):

$$Z_{yx} = (w\,e^{i\delta})\,Z^r_{y'x'} - (g\,e^{i\varphi})\,Z^r_{x'y'}$$

$$Z_{yy} = (r\,e^{i\beta})\,Z^r_{y'x'} + (t\,e^{i\alpha})\,Z^r_{x'y'}$$

Thus, the elements Z_{yx}, Z_{yy} are a linear combination of the regional fields and the distortion parameters, giving them no reason to drop as was assumed for the elements Z_{xy} and Z_{xx}. This means that the pairs of the tensor element columns approach:

$Z_{yy}/Z_{xy} >> 1$ and $Z_{xx}/Z_{yx} << 1$

and the maximal twist and shear angles are therefore valid (eq.6.7).

Eq.(6.15) implies that each pair of phase deviations β, δ and α, ϑ (with regard to polarization mode Y'X' and X'Y', respectively) should be equal in magnitude.

Thus from eq.(6.15), the following is achieved for the phase deviations:

$$
\begin{array}{l}
if\ \theta \geq 0 \quad \rightarrow \beta \approx \delta \quad,\quad \alpha \approx \vartheta \\
if\ \theta < 0 \quad \rightarrow \quad |\beta - \delta| \approx \pi,\ |\alpha - \vartheta| \approx \pi
\end{array}
\tag{6.16}
$$

for $\frac{-\pi}{2} < \theta \leq \frac{\pi}{2}$.

In words, the phases of the distorted tensor elements $Z_{x'x'}$ and $Z_{y'x'}$ (of the magnetic field

component induced in the x' direction) have the same magnetic distortion effect. Such case is also true for the phases of the tensor elements $Z_{x'y'}$ and $Z_{y'y'}$ (of the magnetic field induced in the y' direction).

The equal phase deviation is the magnetic distortion condition to validate the DC channeling assumption. Since this condition arises from the zero-solutions of the tensor elements, which implies the extreme (or ideal) current channeling effect, the phase distortions of the corresponding pair of tensor elements (β, δ and α, ϑ) approaching the same values can be considered a measure of the amount of current channeling.

The following section shows that the physical characteristics derived here lead to a telluric distortion condition for the validity of the channeling model, too.

6.1.5 Impedance in the regional coordinate system

Considering eq.(6.16), the quotient between each pair of elements of the impedance tensor columns in the regional coordinate system (eq.(6.4)) will be real in the form:

$$\frac{Z_{xx}}{Z_{yx}} = \frac{r}{w}e^{i(\beta-\delta)} = \frac{r}{w}\cos(\beta-\delta)$$

$$\frac{Z_{yy}}{Z_{xy}} = \frac{t}{g}e^{i(\alpha-\vartheta)} = \frac{t}{g}\cos(\alpha-\vartheta)$$

The subscript x,y refers now to the regional coordinate system. The cosine functions take the values ± 1 since the phase deviations are equal or they differ by $\pm\pi$.

By taking eq.(6.15) into account these quotients are equivalent to:

$$\frac{Z_{xx}}{Z_{yx}} = \frac{r}{w}sign(\theta) = \tan(\theta)$$

$$\frac{Z_{yy}}{Z_{xy}} = \frac{t}{g}sign(\theta) = \cot(\theta)$$

Then, the phase deviations of the telluric vectors (eq.(6.5)) in terms of the complex distortion matrix and thereby the distortion twist (β_t) and shear (β_e) angles are:

$$
\begin{aligned}
\beta_e + \beta_t = \arctan\left(\frac{Z_{yy}}{Z_{xy}}\right) &= \arctan\left(\frac{t}{g}sign(\theta)\right) &= sign(\theta)\frac{\pi}{2} - \theta \\
\beta_e - \beta_t = \arctan\left(\frac{Z_{xx}}{Z_{yx}}\right) &= \arctan\left(\frac{r}{w}sign(\theta)\right) &= \theta
\end{aligned}
\tag{6.17}
$$

From Eq.(6.17)[4] shear is maximal:

$$\beta_e = \frac{sign(\theta)\pi}{4} \tag{6.18}$$

and twist depends solely on the local azimuth:

$$\beta_t = \frac{sign(\theta)\pi}{4} - \theta \tag{6.19}$$

---

[4] *The solution for the first equation is obtained from the relation: $\theta + \arctan(\cot\theta) = sign(\theta)\frac{\pi}{2}$ for $|\theta| \leq \frac{\pi}{2}$.*

The maximum shear value (eq.6.18) can also be obtained from the telluric tensor decomposition model (eq.1.20; Groom and Bailey [1989b])) when imposing that

$$\left(\frac{Z_{xx}}{Z_{yx}}\right) = \left(\frac{Z_{yy}}{Z_{xy}}\right)^{-1} \tag{6.20}$$

which results in $\tan(\beta_e) = \pm 1$, thus the sign of shear is unknown. Eq.(6.20) is a necessary condition for the strong current channeling assumption, a result which can be directly seen by introducing the equal ratios between the distortion parameters of eq.(6.15) in the tensor elements (in the regional coordinate system) expressed in terms of them (eq.6.4).

If the maximal shear deformation angle is approached, Groom and Bailey [1989b] gave also a similar expression as found here for the twist (eq.6.19. They inferred this result based on the telluric 2-D distortion model of Zhang et al. [1987], where the sign of $\pi/4$ is given by that of the shear. However, their local strike is indeterminate by $\pm\pi/2$, while the local strike derived here represents the azimuth of the horizontally elongated conductor.

Further details with regard to the analogies existing between the telluric decomposition model and the model presented here can be seen in Appendix B.1.

6.1.6   Channeling model of sub-parallel conductivity structures

For small θ ($<20°$; i.e., the regional strike is similar to the local azimuth) it is seen that the telluric deformation takes the approximate favored direction inferred from the boundary conditions (cases $\mathbf{A}, \mathbf{B}$) for a highly conductive horizontally elongated thin body (with azimuth along x) embedded in a resistive host, implying that the distortion parameters of the superposition model (eq.6.11) are:

$$r \;\; << \;\; w \;\; \text{and} \;\; t \;\; >> \;\; g \quad (\text{from eq.6.17 for small } \theta^5),$$

conditions which are inferred directly from eqs.(6.17). For non-negligible anomalous magnetic fields, the magnetic distortion is seen mostly by the TE-polarization mode, i.e, the anomalous magnetic field (B_y) is approximately perpendicular to the azimuth of the elongated conductor (case B). This distortion is contained in the magnetic parameter γ which reflects a rotation of the regional B_y toward x (Smith [1997]). Since the magnetic effect is not manifested in the TM-polarization, the regional B_x field shows no apparent rotation toward y and thus ε is negligible. Then:

$$0 \;\; \approx \;\; |\varepsilon| \;\; << \;\; |\gamma| \quad (\gamma \text{ is proportional to the rotation of } B_y^r \text{ towards } x)$$

Taking this preference distortion directions into account and recalling eq.(6.4) of the superposition model (section 6.1.1), the following equations for the measured impedance elements Z_{xx} and Z_{yx}, related to the TM-polarization mode (YX), are approached (for small θ):

---

[5]For greater $\theta(> \pi/4)$ the preference telluric deformation is reversed, thus $g \leftrightarrow w$, $t \leftrightarrow r$.

Because the magnetic parameter $\varepsilon \approx 0$,

$$
\begin{aligned}
Z_{xx} &= (c - \varepsilon Z_{xy}) \, Z^r_{yx} = (re^{i\beta}) Z^r_{yx} &\approx& \quad c Z^r_{yx} \\
Z_{yx} &= (1 - \varepsilon Z_{yy}) \, Z^r_{yx} = (we^{i\delta}) Z^r_{yx} &\approx& \quad Z^r_{yx}
\end{aligned} \tag{6.21}
$$

with $r \ll w$ and $w = 1$ then $r = |c| \ll 1$.

The tensor elements related to the TE-polarization mode (XY) remains with the general telluric and magnetic distortion model:

$$
\begin{aligned}
Z_{xy} &= (1 - \gamma Z_{xx}) \, Z^r_{xy} &=& \ (\, g e^{i\vartheta}) Z^r_{xy} \\
Z_{yy} &= (b - \gamma Z_{yx}) \, Z^r_{xy} &=& \ (te^{i\alpha}) Z^r_{xy}
\end{aligned}
$$

with $t \gg g$.

This means magnetic effects are distinguishable only by the elements Z_{xy} and Z_{yy}, which corresponds to the TE-polarization mode.

Greater $|b/c|$ values indicate a smaller angle θ ($b = c \cdot \tan(\theta)$; Appendix B.1), while greater $|\gamma|$ indicates an increasing magnetic distortion. $\gamma < 1$ means that the anomalous magnetic field has smaller magnitude than the regional field (Smith [1997]).

If the channeling model is approached (for DC-currents), then is possible to remove the strong current channeling affecting the impedances and thereby obtain the expected regional tensor. In the special case when $\theta = 0$ and provided that the total fields are not measured on the near end of the elongated anomaly, the magnetic effect will not be detectable (i.e.,$\gamma, \varepsilon = 0$) because the horizontal anomalous magnetic field in the strike direction is absorbed in the regional component parallel to it (the indeterminacy of the off-diagonal elements of the magnetic matrix D_m). On the other hand, the anomalous electric field will produce no rotation of the regional fields (i.e., zero twist and shear). A tensor decomposition does not make sense in this case.

6.1.7 Regional strike and regional 2-D tensor determination

For the distorted tensor in the regional coordinate system the following conditions are to be considered to validate the model assumed in the current channeling analysis:

(1) Under DC-limits, the telluric (b, c) and magnetic distortion (ε, γ) parameters should be frequency independent.

(2) The distortion phase deviations should take the form $\alpha \approx \vartheta$ (or $|\alpha - \vartheta| \approx \pi$) and $\beta \approx \delta$ (or $|\beta - \delta| \approx \pi$), as well as the telluric angles twist and shear approaching eqs.(6.19) and (6.18), respectively.

The first condition validates the assumption of galvanic distortion and the second condition is met in the case of strong current channelling. The latter was deduced from the condition of negligible tensor elements Z_{xx} and Z_{xy} in the local coordinate system (eq.6.15), which implies equal phase deviations due to the magnetic distortion (eq.6.16) as well as a maximal shear deformation angle and a twist depending solely on the local azimuth. If case (2) is

approached, then (1) must be achieved, too.

Through the search of the minimum standard deviation of each averaged distortion parameter in the frequency range (condition (1)), a regional strike (θ_r) independent of frequency can be found.

Through the search of the minimal difference of distortion phase pairs and twist and shear values (condition (2)) by frequency, a regional strike for single frequencies can be found.

If the frequency independent regional strike is similar to the frequency dependent ones, then one can conclude that the measured impedances are in fact affected by strong galvanic current channeling. Once the regional strike is found, the regional impedance is obtained from eq.1.28 by using the exact solutions given by Smith (1997) for the distortion parameters (eq.1.26 and 1.27).

A more rigorous analysis of the frequency dependent strike angle determination is presented in Appendix B.3.3.

6.1.8 3-D induction strength and frequency independent strike angle

A measure of the departure from the 2-D superposition model hypothesis −assigned to as "3-D induction strength"− can be based on the frequency independent distortion assumption (valid for DC-current). This is simply the standard deviation of the distortion parameters averaged in the period band, which is dependent of the tensor coordinate system. Thus, the minimal standard deviation value encountered for the coordinate system gives the regional strike of the superposition model. The function to minimize (by rotating the tensor in step strike angles) is:

$$
\partial g^2 = \frac{\sum\limits_{i=1}^{N} \left[\left(b^i - \bar{b}\right) + \left(c^i - \bar{c}\right) + \left(\varepsilon^i - \bar{\varepsilon}\right)^2 + \left(\gamma^i - \bar{\gamma}\right)^2 \right]}{4(N-1)}
\tag{6.22}
$$

The magnetic γ, ε and telluric distortion parameters b, c are obtained from eqs.(1.26) and (1.27), respectively.

A value $\partial g^2 = 0$ validates the ideal superposition model, whereas greater values indicate the departure from it, thus reflecting an increment of 3-D inductive effects.

A 3-D induction effect arises obviously from 3-D conductivity anomalies. Such a structure alone can produce the 3-D induction if its scale is larger than the skin depth of the EM-fields induced in it (i.e, a regional 3-D anomaly). The 3-D inductive effect can arise however by small scaled and shallow 3-D bodies (i.e., smaller than a skin depth in terms of the anomaly), provided that a regional conductivity structure is placed electrically near to it in order to produce an inductive coupling between both structures.

In this context, the parameter ∂g^2 is a measure of the strength of the 3-D induction, either due to regional 3-D conductivity anomalies and/or a coupling between small 3-D anomalies and regional 1-D/2-D conductivity structure(s).

Further explanations can be seen in Appendix B.3.1.

6.1.9 Local azimuth

In the assumed regional coordinate system, the angle between the regional and local structures is:

$$\theta = sign(\beta_e)\frac{\pi}{4} - \beta_t$$

and the local azimuth with respect to the measured coordinates is:

$$\theta_l = \theta^r - \theta \tag{6.23}$$

where θ^r is the regional strike defined positive c.w. with respect to the measured coordinate system.

The local azimuth coincides with the elongated conductor orientation (x) for the vanishing electric field component aligned with it. Thus in the local azimuth coordinates, the tensor elements approach:

$$\frac{|Z_{xx}|}{|Z_{yx}|} < \frac{|Z_{yy}|}{|Z_{xy}|}$$

and the local azimuth defines the correct strike of the elongated conductor.
The local azimuth error at a single frequency is:

$$\Delta\theta_l = |\beta_e - sign(\theta)\,\pi/4|\,.$$

The complete derivation of the azimuth and its error can be seen in Appendix B.3.2, as well as the determination of a multiple frequency azimuth.

6.1.10 Channeling misfit

A function to measure the departure from the channeling model hypothesis, expressed in terms of the condition of equal magnitude of distortion ratios (eq.6.15) and phase deviations (eq.6.16) of the elements of the distortion matrix C (eq.6.2) is:

$$CM = |(r/w) - (g/t)|^2 + |\sin(\beta - \delta)|^2 + |\sin(\vartheta - \alpha)|^2$$

. The channeling misfit (CM) can also be expressed in terms of the impedance elements in the assumed (regional) coordinate system (eq.6.20; Appendix B.3.3):

$$CM = (|Z_{xx}|\,/\,|Z_{yx}| - |Z_{xy}|\,/\,|Z_{yy}|)^2 + |\sin(\phi_{xx} - \phi_{yx})|^2 + |\sin(\phi_{xy} - \phi_{yy})|^2$$

For noise-free data, the approach of 0 by the function CM would validate the ideal model assumed in the current channeling analysis, and the local azimuth (eq.6.23) would reflect the elongated conductor orientation. Greater values would indicate a weaker DC channeling effect.
For noisy data, the channeling misfit is normalized by the data error (appendix B.3.4).

6.2   Example with synthetic data

The theory was tested with a 2-D anisotropic model and the response was computed with the forward finite difference code developed by Pek [1994]. The thin elongated conductors are conceived as electrical macro-anisotropies. The horizontal anisotropy can have any strike different from the regional model. The proposed distortion analysis procedure will serve to investigate if the anisotropic structures can be recognized as attractors of current channeling. The regional 2-D model simulates the ocean structure of the Central Andes zone, considering roughly a similar conductivity structure beneath the ocean as that from the Pica profile 2-D model (Echternacht [1998]). The ocean bathimetry, the grid definition and the anisotropy factor was taken from the modeling study of the near Pacific ocean investigation area at latitude 21°S (J. Beike, in preparation).

In the model, an anisotropic body is embedded in a 500 Ωm resistivity space, extending between 500 m and 9 km depth (the shallow block in the centre of the model; fig.6.6). It is located 30 km away from the regional conductivity contrast. The highly conductive ocean reaches a maximal depth of 4 km and is also embedded in the 500 Ωm space, followed below by a resistive block of 4000 Ωm extending from 8 to 65 km depths. The bottom half space of the model is a low resistivity layer of 10 Ωm located beneath 300 km of depth, simulating a conductive upper mantle.

Inserting a more resistive block beneath the ocean should lead to an increase in the continental upper crust currents induced by the conductive ocean (e.g., Mackie et al. [1996]), which should lead as well to an enhancement of current in the anisotropic body. The horizontal
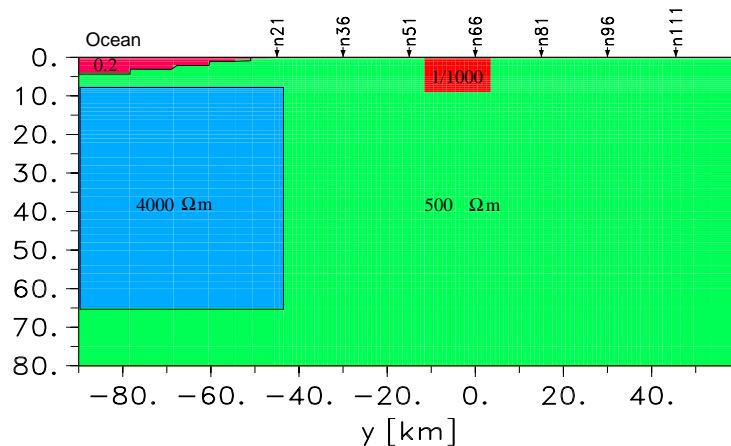
Figure 6.6: 2-D model with horizontal anisotropy of factor 1/1000 Ω.m in the block located in the centre of the model. The site names for which the results of the channeling analysis at two anisotropy directions of 30° and 10° azimuth are shown are indicated on the top (figs. 6.7, 6.9).

anisotropy contrast is 1/1000 Ωm. The anisotropy azimuth was set differently. Results for a 30° and 10° c.c.w rotation with respect to the regional coordinate system are shown. Thus the direction of high conductivity is oriented 30° or 10° c.c.w. with respect to the regional strike.

The procedure for investigating the channeling effect has been based on the assumption of frequency independent distortion parameters (section 6.1.7) treated in the period band 50-8000 s. The regional strike was determined for single sites thereof, where a 2% error proportional to the tensor element magnitude was added on the model impedance. The degree of induction effect is estimated with the 3-D induction strength parameter (section 6.1.8) and as is the validity of the current channeling assumption with the channeling misfit parameter (section 6.1.10). The calculation of the local azimuth (section 6.1.9) reveals whether or not the strike of the high conductivity anisotropy, provided that the DC channeling hypothesis is approached.

Model with 30° anisotropy direction

At an anisotropy direction of 30°, the maximal 3-D induction strength is seen for the sites above the anomaly, as well as a minimal channeling misfit (at $[-10, 5]$ km in fig.6.7). This reflects the current channeling effect produced by the anomaly, where induction effects are not negligible. The real regional strike (0°) is recovered at almost any site, except at one site located between the ocean and the anomaly (at -40 km) which also shows strong channeling effect.

Above the anomaly, the local azimuth of the DC channeling analysis recovers the anisotropy direction for periods shorter than 300 s, where a maximal shear deformation (45°) is nearly achieved (fig.6.8). Also, the range of the frequency dependent regional strikes under the channeling assumption (see App. B.3.3 for calculation details) remains near 0° at short periods, coinciding with the found frequency independent strike angle. Thus the model hypothesis of local horizontally elongated conductors is satisfied at short periods, whereas an induction effect is clearly observed at periods >100 s: the telluric deformation is reversed as the magnetic distortion parameters. A greater phase departure for the elements pairs yx and xx is also observed at longer periods, thus indicating non-validity of the model hypothesis at greater penetration depths. The magnetic effect of the TM-polarisation mode (ε big) is notorious in this region.

At the sites to the west and east of the anomaly the Swift angle[6] is relatively frequency independent with a 0° value, thus pointing to the regional strike. At the 0° strike angle all distortion parameters are zero as well as twist and shear deformation angles. This means that the anisotropic anomaly can not be detected. In contrast, when determining the regional strike by the frequency dependent channeling methodology (app. B.3.3), a regional angle around the $35 - 45°$ is found, resulting in a 0° local azimuth as well as in a high shear deformation angle, being maximal to the west, in the direction of the highly conductive ocean[7]. The channeling misfit at the $35 - 45°$ strike angle is small for the sites located between the ocean structure and the anomaly, thus reflecting an increment of currents in this region due to the ocean.

---

[6]The Swift angle (Swift [1967]) indicates the coordinate system of the tensor where the sum of its diagonal elements are minimum. In an ideal 2-D case, the diagonal tensor elements vanish in the 2-D coordinate system.

[7]In a pure 2-D model twist and shear angles are always zero.

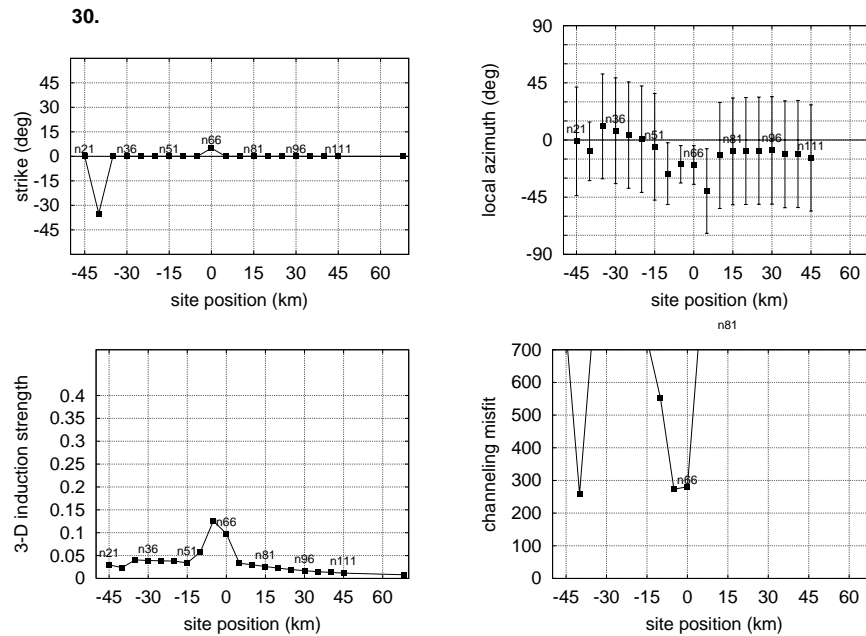*Figure 6.7:* Parameters as a function of the site location of the current channeling analysis for the 30° anisotropy model. *Left:* The graphs above show the frequency independent regional strike angles determined for single sites, found for the minimal 3-D induction strength parameter averaged over all periods (*bottom graphic*). *Right:* The averaged current channeling local azimuth for single sites, with errors (in app. B.3.2) proportional to the channeling misfit (*bottom graphic*). The highest distortion is seen above the anisotropy ([−10, 5] km), where the characteristics of the model of elongated conductors is observed at short periods (< 300 s).

Model with 10° anisotropy direction

Some similarities and differences in the results of the −30° and −10° anisotropy models are observed (fig.6.9). In the −10° anisotropy model, the maximal 3-D induction strengths are seen for sites located just above the anomaly, as well as a minimal channeling misfit. This indicates the presence of strong current channeling and an inductive effect which is higher at the -10° anisotropic anomaly (greater 3-D induction strengths for a 0° fixed azimuth; fig.6.11) than was seen for the 30° anisotropy. Also, the current channeling misfit, estimated at the corresponding angles of the minimum 3-D induction strength, observed at sites located between the ocean and the anisotropic body, are smaller than in the 30° anisotropy model (fig.6.9). This reflects a stronger current channeling in the -10° anisotropy model in this region.

The frequency independent strike angles reflect the regional strike for the sites east of the anomaly (>0 km in fig.6.9), where no current channeling effect is detected. However, at the sites located between the ocean and the anisotropic anomaly, the frequency independent strike angle recovers not the model strike of 0°, but rather an angle close to 45° (due to the stronger inductive effect mentioned above, fig.6.11), which coincides with the determination of the frequency dependent strike. Above the anomaly the strikes do not differ much from the model. They are also rather close to the frequency dependent strike angles. These observations lead to the conclusion that angle determination by minimum 3-D induction strength can not recover the regional strike when the current channeling is too strong and affected by induction effects.
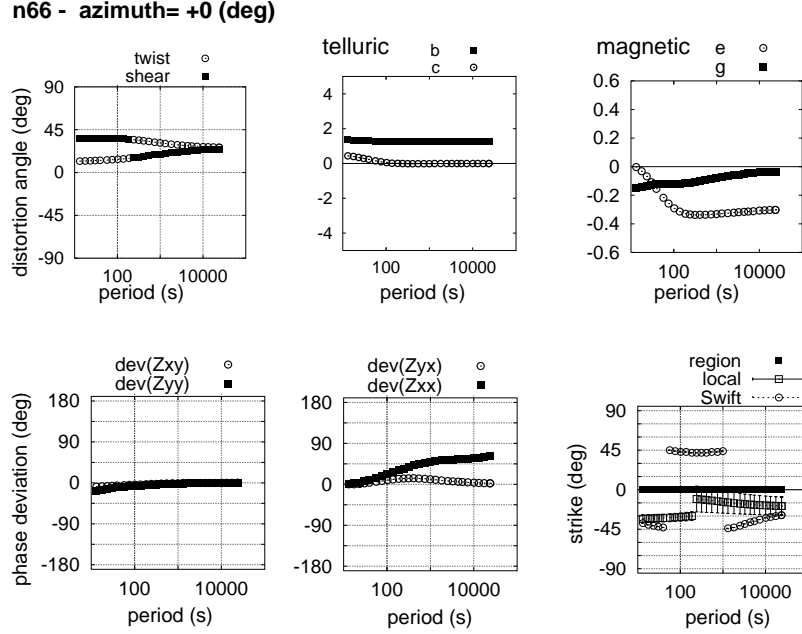
Figure 6.8: Illustration of the distortion parameters considered in the channeling analysis for site n66, located above the 30° anisotropic body. *Top:* The graphics from left to right show the twist and shear deformation angles, the telluric and magnetic distortion parameters ($g = \gamma$, $e = \varepsilon$), respectively. *Bottom:* From left to right are shown the phase deviations of each pair of tensor elements. The right plot shows the *regional* strike, the current channeling *local* azimuth and the conventional *Swift* angle. The local azimuth for periods <300 s reflects the anisotropy direction of the highest conductivity value.

As in the 30° anisotropy model, the telluric deformation angles for the fixed 0° strike angle vanish at the sites located to the east and west of the anomaly. The magnetic parameters, in contrast, are not necessarily close to zero, as is reflected in greater 3-D induction strengths.

Above the anomaly, the current channeling local azimuth could recover the true anisotropy direction for periods <1000 s. As an example, the distortion parameters for site n66 (above the anomaly) are illustrated in fig.6.10 for the 0° fixed strike angle. The distortion characteristics of the *model of sub-parallel conductivity structures* described in section 6.1.6 are observed at the short periods:

1) Approximately equal and maximal twist and shear deformation angles.
2) Vanishing TM-mode telluric (c=0) and magnetic (ε=0) distortion parameters.
3) Great TE-mode telluric (b>>0) and magnetic ($\gamma \gg 0$) distortion parameters.

The frequency dependent magnetic parameters observed at periods >1000 s reflect an induction effect at the corresponding penetration depths. The reversal in the telluric deformation (twist and shear) and the magnetic parameters at 1000 s indicate a change in the direction of the current flow. All these observations are due to the inductive coupling effect exerted between the ocean and the anisotropic block, since they are the only shallow conductive
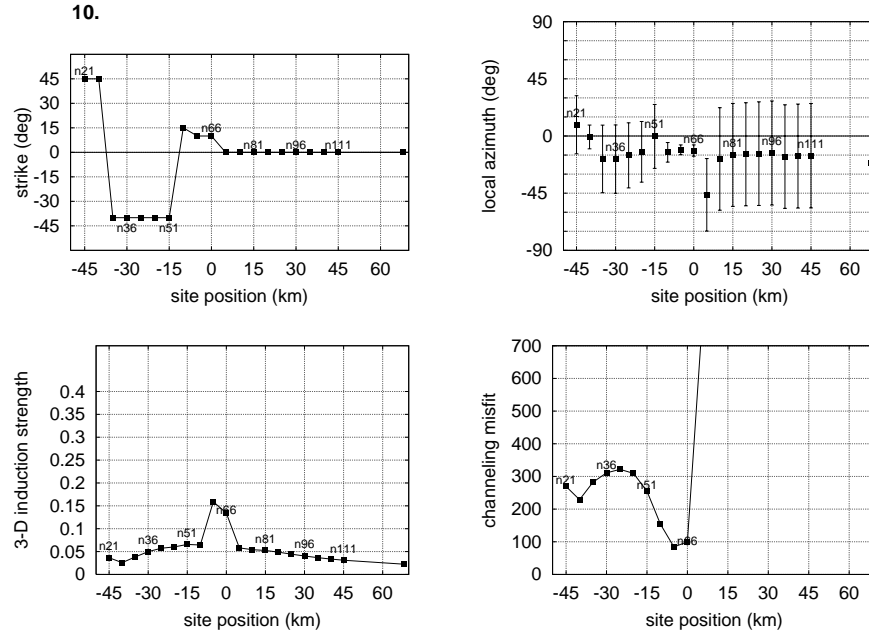
Figure 6.9: Parameters as a function of the site location of the current channeling analysis for the $10°$ anisotropy model. Graphic explanations are as in fig.6.7. The highest distortion is seen above the anisotropic body (at $[-10, 5]$ km), where the channeling assumption becomes valid at periods <1000 s.

bodies present in the model[8]. The resistive block beneath the ocean has no influence on the change of direction of the current flow. The effect of the resistive block is manifested by a mere increase of induction above the anomaly with respect to the model without this block (not shown here).

Conclusions

From these results we can conclude that a horizontally elongated conductor oriented similarly to the regional axis increases the current channeling and magnetic effects in the presence of a nearby regional high conductivity zone. This means for the model example shown here that the current flow produced by the coupling effect between the highly conductive ocean and the anisotropic body are more strongly channeled if the two structures are sub-parallel to one another. The distortion characteristics postulated in section 6.1.6 for the channeling model of sub-parallel structures has been identified in the $10°$ anisotropy model for sites located above the anomaly and at periods <1000 s. The equal phase deviations between the pairs of the tensor element columns are however not achieved, due to the inductive effect.

The anisotropy can be identified with a current channeling effect. The local azimuth of the channeling model (section 6.1.9) recovers the anisotropy direction for sites located above the anomaly. Meanwhile the regional strike is recovered outside the strong current channeling region.

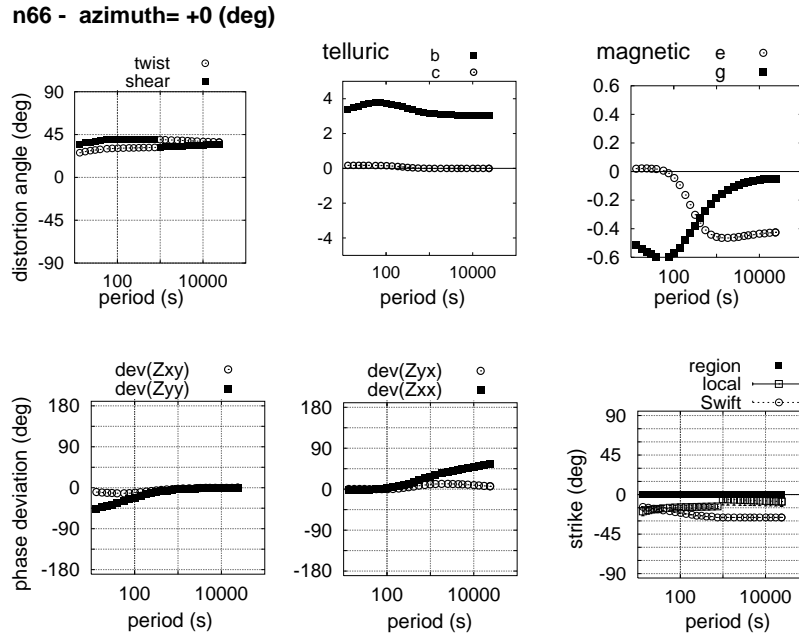[8]The skin depth at 1000 s is about 13 km for a surface observation point located above the anisotropic body

Figure 6.10: Illustration of the distortion parameters considered in the channeling analysis for site n66 located above the 10° anisotropic body. Graphic explanations are as in fig.6.8. The *local* azimuth for periods <1000 s reflects the anisotropy direction of the highest conductivity value.
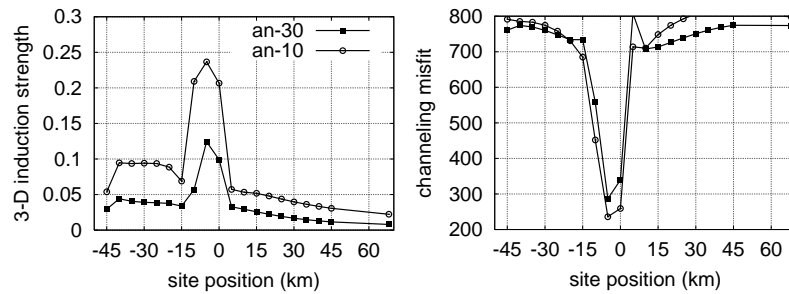

Figure 6.11: 3-D induction strength (*left*) and channeling misfit (*right*) of the -30° and -10° anisotropy models (an-30, an-10). Procedure performed in the whole period band (10-10000 s) for the impedance tensor in the 0° (2-D model) strike angle. The greater 3-D induction strengths in the -10° anisotropic body (at position [−10, 5] km) reflect a stronger inductive coupling between this and the ocean structure.

6.3   Analysis in the measured area

The current channeling analysis introduced in section 6.1 has been applied to the MT data. First the single site regional strikes are determined to verify if a consistent angle −or one similar to that derived from the tensor decomposition methods− is found (section 6.3.1), as well as to permit a 3-D image of the interpolated site distortion parameters in the coordinate system of the strike angle found by this procedure (section 6.3.2). The 3-D images tested at different coordinate systems permit quantification of the current channeling effect and identification of the anomalous high conductivity structures of the region. The single site local azimuths of the current channeling analysis (i.e., the elongated conductors azimuth) have been determined in the Coastal Cordillera and Precordillera, where the hypothesis is better approached (section 6.3.3).

6.3.1   Regional strike determination

The procedure to find the single site strike angles is based on the assumption of a frequency independent distortion (section 6.1.7). Thus the minimal 3-D induction strength found at a selected period band defines the regional strike (section 6.1.8). The method can also be extended to a multiple site analysis, by a minimum 3-D induction strength estimated from multiple sites at the selected period band. The function to minimize is that which account for possible trends along the period range (appendix B.3.1).

In fig.6.12 the multiple site regional strikes found are shown for the same period bands as selected for the telluric and magnetic tensor decomposition (fig.5.8), and the same site arrays are considered (table 5.1). No consistent strike angle can be seen for the whole region. However, the strike angles are near -30° for many sites located between the coast and the Longitudinal Valley, especially at the long period band solution.
The similarities between the results obtained by this method and that of the telluric and magnetic decomposition (section 5.2.2) can be seen in the near 40° angles at some locations.
  As was shown in the anisotropy model example (section 6.2), the regional strike cannot be recovered in the regions affected by strong channeling effects. The current channeling analysis shown in the next section verifies the existence of such distortion effects, thus explaining the inconsistence among the regional strikes found in the measured area. But a qualitative picture of the anomalous conductivity structures present in the region is recovered (section 6.3.2).

6.3.2   3-D image of the distortion: channeling misfit, 3-D induction strength and magnetic effects

Following the same procedure for the current channeling analysis as described in the synthetic data example (section 6.2) for testing the hypothesis, the short and long period data have been analyzed at different strike angles. Specific distortion parameters for single sites are estimated and then all sites are interpolated for a 3-D image.
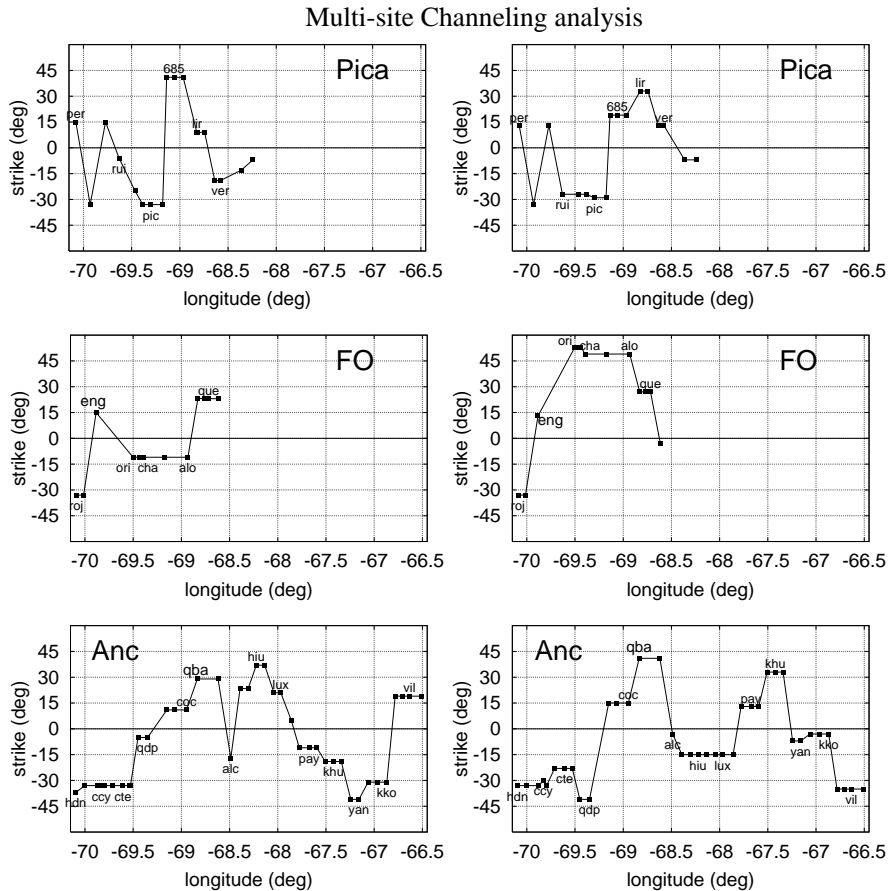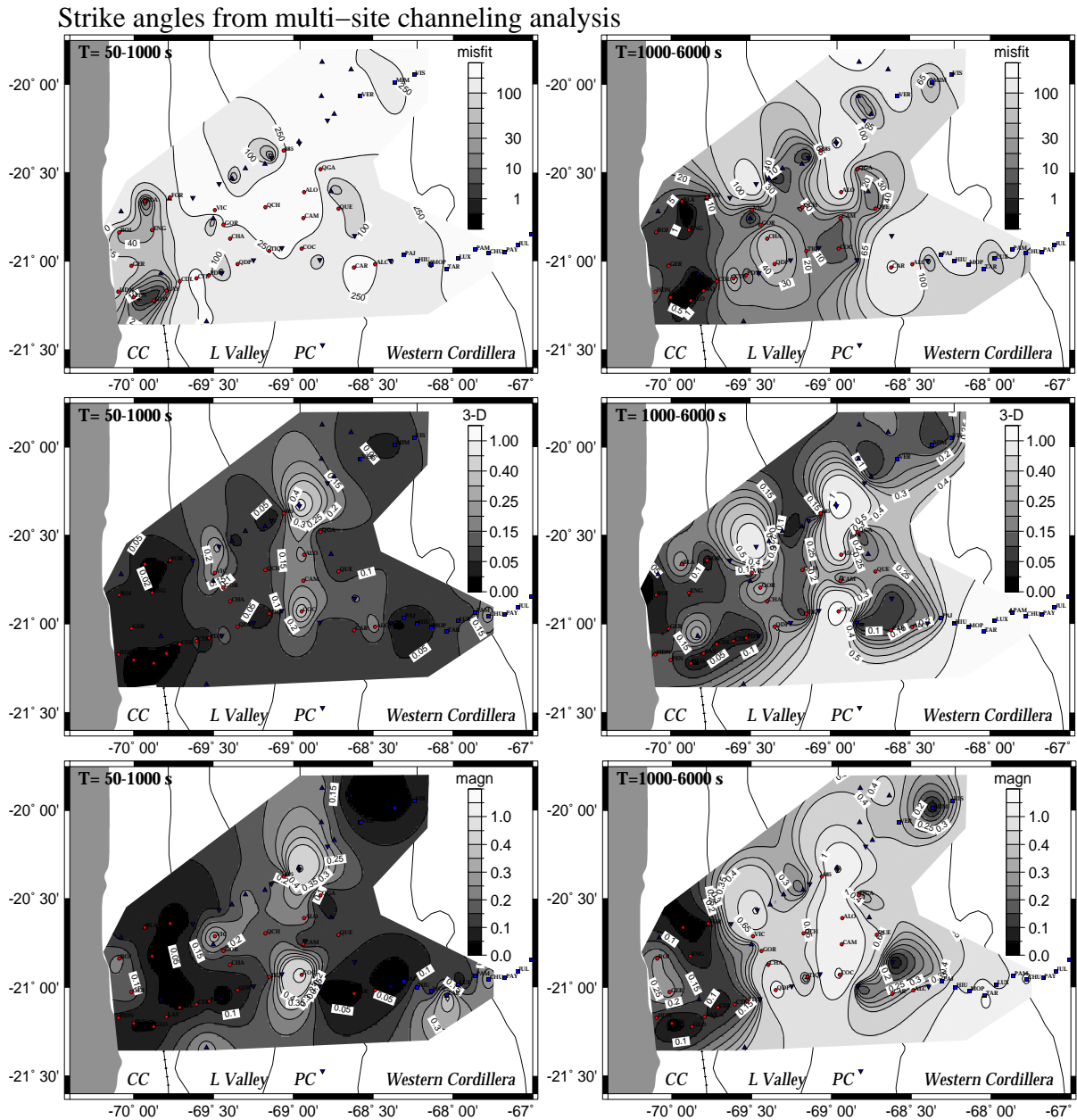
Multi-site Channeling analysis

Figure 6.12: Regional strike directions for the sites along the Ancorp profile (*top*), Pica profile (*bottom*) and the sites in between (*center*). The solution is obtained by the telluric and magnetic tensor decomposition for fixed multiple site strike angles of the minimal period averaged 3-D induction strength (section 6.1). *Left:* Procedure performed in the period range 50−1000 s. *Right:* Procedure performed in the period range 1000−8000 s.

First, the channeling analysis for the MT data rotated to the minimum 3-D induction strength regional strike are presented (fig.6.12). The channeling misfit (section 6.1.10) and standard 3-D induction strengths (section 6.1.8) have been calculated for each site at the short (50−1000 s) and long (1000−6000 s) period band. The interpolated parameters are shown as contour plots in fig.6.13. Also, the interpolated single site magnetic distortion parameters averaged over the period bands of the superposition model (γ, ε; eq.6.1.1) are shown. The magnetic parameters reflect the deviation of the regional magnetic field from its coordinate system due to anomalous DC magnetic fields caused by the 3-D structures (Smith [1997]). The section is limited to the east up to longitude 67.5°W because no sites in the Altiplano to the north of Ancorp are available. Thus the most eastern Ancorp profile data have been excluded from the contour plots.

According to the synthetic data example of section 6.2, a superposition model[9] was assumed in general for sites having a 3-D inductive strength below or near the value 0.05, whereas the maximal values indicative of induction effects (associated with a 3-D conductivity anomaly

---

[9]Superposition model: a regional 2-D model overlain by shallow local 3-D structures.

Strike angles from multi–site channeling analysis

Figure 6.13: Interpolated site averaged data of the current channeling analysis (section 6.1). *Left:* Procedure performed in the period range 50−1000 s. *Right:* Procedure performed in the period range 1000−6000 s. *Top row:* Contour plots of the *channeling misfit* (appendix B.3.4). Values >100 (in white) indicate the absence of current channeling effects. Light gray identifies areas of weak channeling or with currents exceeding the DC-limits. Strong current channeling is presented in dark gray. *Center row:* Contour plots of the *3-D induction strength*. Values <0.15 (in dark) support the assumption of a regional 2-D model, while greater values (light-gray-white) identify areas affected by 3-D induction. *Bottom row:* Contour plots of the interpolated site averaged *magnetic distortion parameters*. Usually large values (light-gray-white) are associated with induction effects (i.e., high 3-D induction strengs). MT Data have been rotated to the strike angles of the minimum period averaged 3-D induction strength (in fig.6.12).

beneath or near the site) were found by surpassing 0.1-0.15 (figs. 6.7 and 6.9). I will refer to values 0.1-0.15 as the *tolerance level* of the galvanic distortion assumption[10]. The maximal 3-D induction strengths were seen at sites located just above the local anomaly (the anisotropic body in fig.6.7), where magnetic distortions were also greater. Thus the 3-D images of the 3-D induction strengths and magnetic distortion parameters can be a tool to identify anomalous conductivity bodies qualitatively in the studied region. The current channeling misfit parameter can give insights on the geometry of the anomaly, specifically, if the anomaly can be considered as horizontally elongated conductors.

As has been shown in section 6.2, the channeling effect increases in regions between two conductors. Moreover, it becomes significant by smaller axial angle departures between the elongated anomaly and the regional structure (e.g., figs.6.9 and 6.7 of the anisotropy model; fig.6.6). In this sense, the channeling misfit is also a tool to identify regions between two sub-parallel conductors.

In our investigation area the superposition model hypothesis is fulfilled at almost all periods for sites located in the near coast (small 3-D induction strength).These data show strong current channeling effects, as seen in the small channeling misfit values. In the top contour plots of fig.6.13, the smallest channeling misfits (in dark grays) are the best representation of galvanic currents due to local horizontally elongated conductors. A more detailed analysis of current channeling in the area is presented in the next section (7).

At the short period band the superposition model fits also with the data of sites located immediately to the east and west of the Precordillera fault system (69°W; fig.6.13), while site data from the Precordillera fault system itself show high 3-D induction strengths at all periods. This reflects the presence of a local anomalous conductivity structure probably associated to the fault system. Strong channeling effects are detected at longer periods between LV and PC of the Pica profile sites (69 - 69.5°W) as well as at several sites distributed along PC, though the channeling misfit in these regions is higher than in the near coast, due to the high 3-D induction strength.

Further interpretations are discussed in a subsequent section (8).

As shown above, current channeling effects due to a model of horizontally elongated conductors is seen to be valid in the Coastal Cordillera at all periods, as well as in the regions to the east and west of the Precordillera fault system (69°W) at long periods. The regional strike inconsistency found between the sites stems from the strong channeling effect, comparable to the anisotropy model (section 6.2).

Under the assumption of a regional 2-D structure, the channeling parameters for all data are first investigated at a fixed azimuth of 0° (i.e., N-S; the measured coordinate system, fig.6.14). By analogy, by assuming a regional structure striking by -8°N, a rotation of −8° is applied to the analysis of all data (fig.6.15). This angle was inferred from the multi-site tensor decomposition of section 5.2.2 (fig.5.8). In general, the 3-D induction strengths are greater at the long period band than at the shorter periods. The exception is the Coastal Cordillera.

The high 3-D induction strengths surpassing the tolerance level (light-gray-white; Figs. 6.13, 6.14 and 6.15; center row) in the Precordillera and to the east are associated with an increase

---

[10]The values 0.1-0.15 assigned to the tolerance level were determined from a set of tests of different 3-D model responses
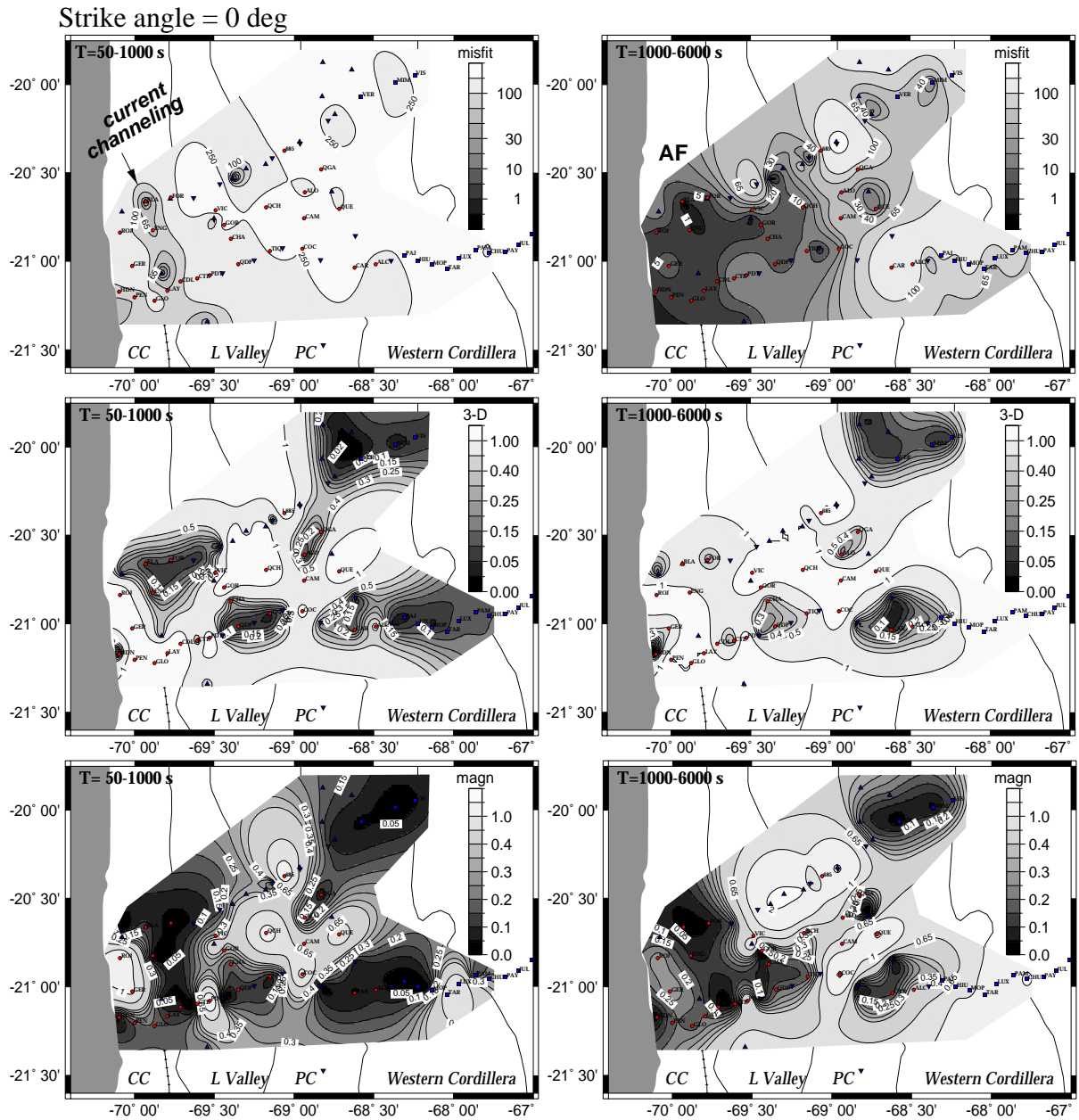
Figure 6.14: Interpolated site average data of the current channeling analysis (section 6.1). *Top* (channeling misfit), *center* (3-D induction strength) and *bottom* (magnetic distortion) graphs as described in fig.6.13. MT Data in the measured coordinate system (N-S). *Left:* Procedure performed in the period range 50−1000 s. *Right:* Procedure performed in the period range 1000−6000 s. **AF**: Atacama fault.
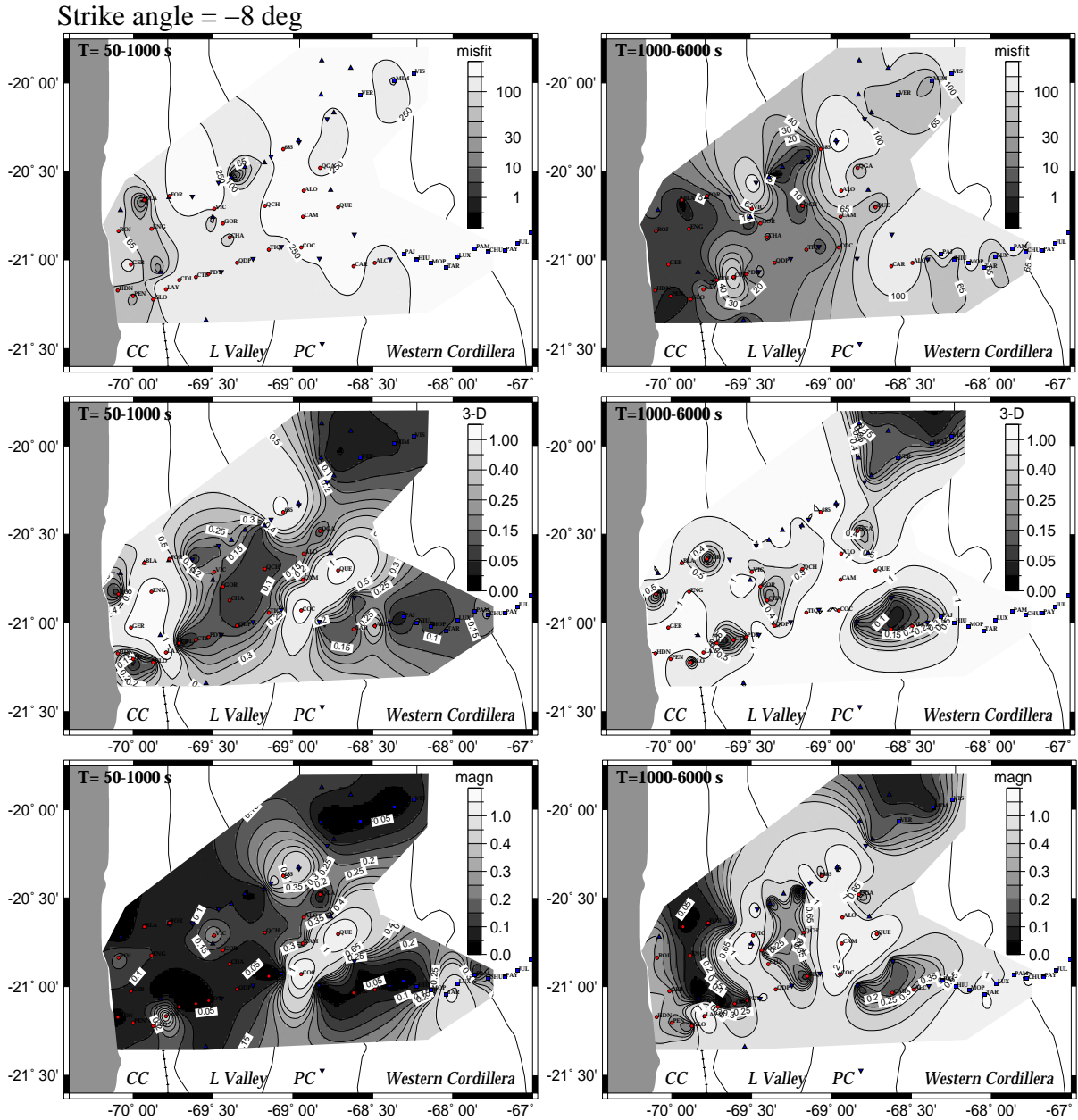
Strike angle = −8 deg

Figure 6.15: Interpolated site average data of the current channeling analysis (section 6.1). Top (channeling misfit), center (3-D induction strength) and bottom (magnetic distortion) graphs as described in fig.6.13. MT data rotated by -8°N. *Left:* Procedure performed in the period range 50−1000 s. *Right:* Procedure performed in the period range 1000−6000 s.

of the magnetic distortion with period (figs. 6.13, 6.14 and 6.15;

bottom). This means that magnetic effects are not negligible and moreover they become significant with the penetration depth.

The presence of frequency dependent magnetic distortion can have different origins, besides elucidating this as an inductive effect due to regional scaled 3-D structures. One possible explanation for the magnetic distortion increasing with period can be the inductive coupling exerted between a deeper conductive layer and shallower 3-D conductivity structures (chapter 8) . Alternatively, for frequency dependent distortion parameters at any specific period band, it could be the case that the measured sites are placed electrically near to the 2-D regional conductivity contrast, provided that this structure is coupled with local small 3-D anomalies. In this case, the assumption of uniform regional fields in which the galvanic distortion hypothesis is based is no longer valid.

In the Altiplano, a plausible explanation an be the observation made with regard to a deep conductive layer producing the inductive effect. The conductivity at depth is inferred directly from the phase data, seen in the phase increment with period (fig. 4.2). Also, 2-D inversion modeling of the Ancorp profile showed that a high conductivity zone extends deep (>15-20 km) beneath the Altiplano (K. Schwalenberg, 2000; and Chapter 9). The models show that the Altiplano anomaly is cut off to the west beneath the Western Cordillera (WC). Thus, the lateral regional conductivity contrast should occur beneath the WC.

Since the 3-D induction strengths at longer periods have also surpassed the tolerance level in the Western Cordillera (WC) data of the Ancorp profile, it can be presumed that the western boundary of the AP-conductor located beneath the WC sites is coupled with local heterogeneities, and is the cause of the induction effect observed in these data set.

Furthermore, the decomposition results, the skew values of the dimensionality analysis and the behaviour of the induction arrows, point to departures from the 2-D superposition model in the Altiplano. To scrutinize if the long period induction effect in the Altiplano stems from a coupling effect between shallow local 3-D structures and a deep 1-D/2-D layered model or from a regional 3-D structure, more measurements are required at latitudes adjacent to Ancorp.

After the *qualitative* interpretation of the anomalous conductivity structures identified in the Coastal Cordillera, Precordillera and Altiplano, where in the first region the model of sub-parallel conductivity structures is found to be appropriate while in the second region the conductivity structures become to be three dimensionally inductive coupled with increasing periods, the following section *quantifies* the geometry of the anomalies where the model hypothesis is valid.

6.3.3   Local azimuth

The current channeling local azimuths of the Ancorp data averaged for single sites at the long period band are shown in fig.6.16, following the format of the figures illustrated by the current channeling analysis applied to syntetic data (section 6.2; e.g., fig.6.9). The local

azimuths of the analysis (i.e., of the elongated conductors) have been estimated for the tensor in the coordinate system of the minimum 3-D induction strength angles (fig.6.16; left). The azimuths are solved best in the Coastal Cordillera region (right in fig.6.16), with angles ranging near 0° (N-S).
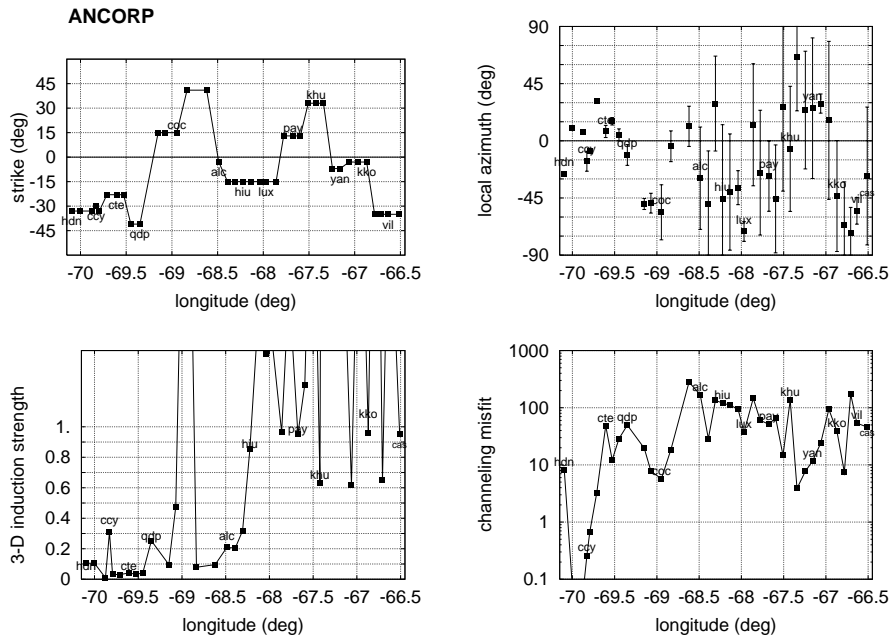
Figure 6.16: Current channeling analysis of the Ancorp profile. *Left:* The *top* graph shows the frequency independent regional strike angles determined for multiple sites, found for the minimum 3-D induction strength in the period band 1000−6000 s. (*bottom graph*). *Right:* The averaged local azimuth for single sites with the propagation errors proportional to the channeling misfit (*bottom graph*).

With the same procedure, the local azimuth of the rest of the sites have been computed, by averaging the values in a determined period band. The local azimuths are presented in the map of fig.6.17, corresponding to the data with angle errors <10° (appendix B.3.2), those which are thus closest to a model of horizontally elongated conductors in the region. The current channeling local azimuths correspond to the near coast data and to the Longitudinal Valley (LV) to the Pica profile, and to some other sites distributed along the Precordillera (PC). In the Coastal Cordillera, the azimuths are obtained from the short and long period data, whereas to the east the current channeling azimuths belong to the longer periods. Most angles fluctuate near 0° in LV and PC regions (69.5-68.5°W).

 Surprisingly, the sites that show strong current channeling effects also have phases of the TE-polarisation mode (i.e., the tangential electric field component) above 90° after rotating the tensor to the local azimuth (fig.6.17). The anomalous phases occur only by the TE-mode for a local azimuth ranging near 0° for most of the sites (the expected regional strike in the Andes), whereas the TM-mode (tangential magnetic field) remains almost unaltered after rotating the tensor. These observations are typical for regions where the *model of sub-parallel conductivty structures* is appropriate (section 6.1.6).
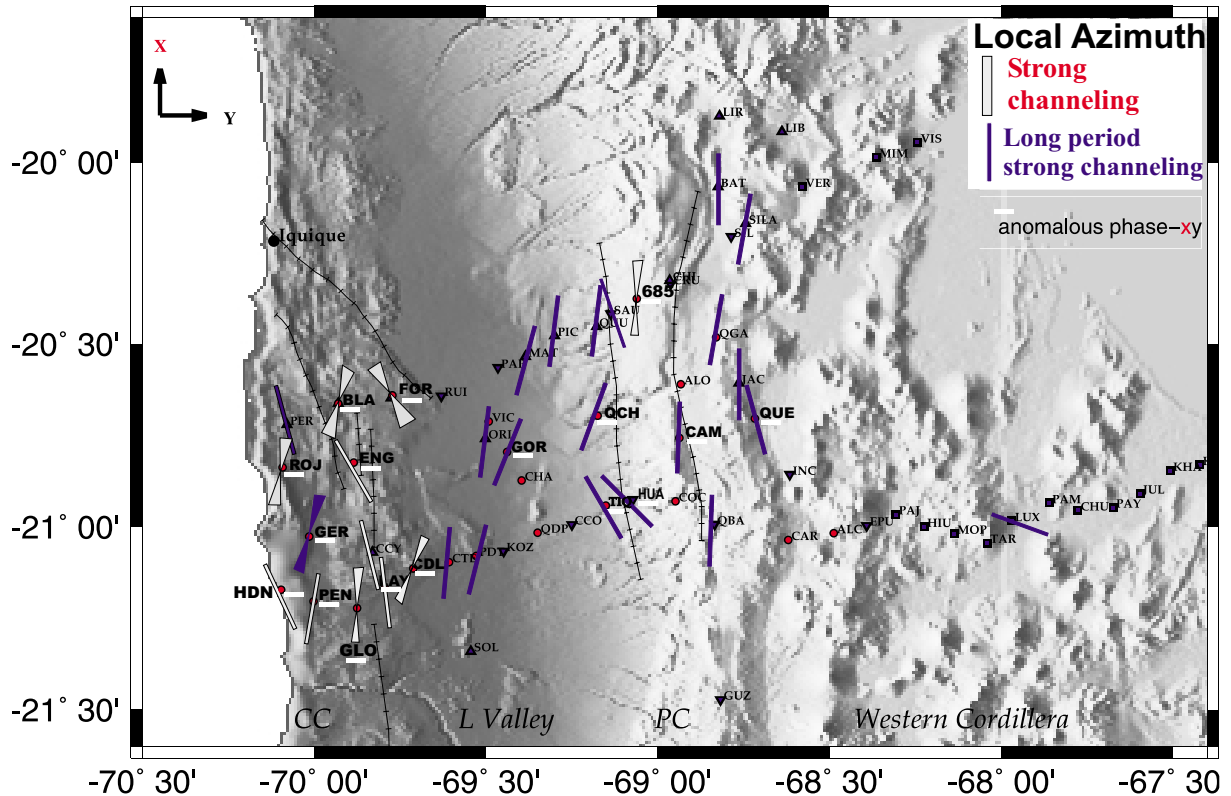
Figure 6.17: Local azimuth according to the current channeling analysis. Light-gray marks the azimuth for data which satisfy the model hypothesis of elongated conductors at all periods. Site data with TE(=XY)-mode impedance phases exceeding 90° after rotating the tensor to the local azimuth are marked in white and labeled in black. The topography (shaded) and the main faults (broken lines) are also shown on the map.

6.3.4 Conclusions

The important results interpreted from the 3-D images (figs. 6.13, 6.14 and 6.15) and from the current channeling local azimuth (fig.6.17) are:

1) a strong current channeling is always observed in the Coastal Cordillera regardless of the tensor rotation, especially at long periods. The model hypothesis of *sub-parallel conductivity structures* is satisfied in the region. The single site local azimuths range between -30°N and 5°N. The electric fields are strongly polarized into the local azimuth direction, where TE-mode phases exceed 90°.

2) In the Coastal Cordillera, at azimuths of 0° and -8°, the high 3-D induction strength identified at short periods together with the small channeling misfit indicate the trend of horizontally elongated conductors, which are oriented in NNW-SSE direction, similar to the Atacama fault system.

3) Strong current channeling effects are also seen at some sites in the Longitudinal Valley and Precordillera at long periods, though the DC-limits have sometimes

been surpassed (high 3-D induction strengths). Under the assumption of the model hypothesis of the current channeling analysis, approximately N-S elongated conductors in the Precordillera fault system are found (fig.6.17). The electric fields of the sites affected are strongly polarized in the local azimuth direction, where TE-mode phases exceed 90°.

4) In the Precordillera, a significant magnetic induction effect (high 3-D induction strengths and magnetic distortion; figs. 6.13−6.15) increasing with period is observed at different tensor rotations, thus reflecting a high conductivity zone. The form of the distortion depends on the MT tensor coordinate system (i.e, the assumed regional strike). At a strike angle of 0° (N-S), the inductive effect extends further to the west in the Longitudinal Valley, reflecting a N-S lateral conductivity variation. At least in the Longitudinal Valley and western Precordillera, an azimuth of -8°N better supports a 2-D regional model at short periods in these regions, while in the Precordillera itself the anomaly can be identified with a high conductivity zone oriented differently, thus with 3-D structures.

5) In the Western Cordillera and Altiplano the 3-D induction strengths increase with period for all considered coordinate systems. These far surpass the 0.15 tolerance level for a 2-D model assumption in the long period band. The magnetic distortion and 3-D induction strength become extremely large at longer periods in the Altiplano, reflecting a high conductivity anomaly at depth.

The following chapters give a more detailed investigation of the anomalies discussed qualitatively in this section, by analysing the distortion characteristics of the data and the responses of 3-D models. The investigation is focused on the Coastal Cordillera region (chapter 7) based on points 1) and 2) above, and on the Precordillera (chapter 8) as motivated by points 3), 4) and 5). The conductivity structures associated with the cause of the distortion of the anomalous TE-phases (> 90°) are also discussed in these chapters.